GEOCHRONOLOGICAL CONSTRAINTS ON YAMBAH AND CHEWINGS-AGED DEFORMATION AT MT BOOTHBY IN THE SOUTH EASTERN REYNOLDS RANGE, CENTRAL AUSTRALIA

Thesis submitted in accordance with the requirements of the University of Adelaide for an Honours Degree in Geology

Daniel Peter Howlett

November 2012

THE UNIVERSITY of ADELAIDE

GEOCHRONOLOGICAL CONSTRAINTS ON YAMBAH AND CHEWINGS-AGED DEFORMATION AT MT BOOTHBY IN THE SOUTH EASTERN REYNOLDS RANGE, CENTRAL AUSTRALIA.

YAMBAH-AGED DEFORMATION, MT BOOTHBY

ABSTRACT

Zircon and monazite U–Pb isotope geochronology combined with structural mapping in the Mt Boothby region in the central Aileron Province in Central Australia has constrained the timing of two tectonically distinct phases of high-grade deformation and metamorphism. The first event (D_1/M_1) occurred at around 1790 Ma and was associated with the emplacement of a bimodal magmatic suite that underwent high-grade deformation prior to the emplacement of voluminous granite also at around 1790 Ma. The timing of D_1/M_1 coincides with the early stages of the Yambah Event, which is widely recognised in the southern Aileron Province, but has not previously been unequivocally shown to be associated with deformation . Subsequent pervasive reworking occurred over the interval 1600-1570 Ma, and was associated with long-lived granulite-grade metamorphism. The timing of this event coincides with the Chewings Orogeny which largely shaped the tectonic geology further west in the Reynolds and Anmatjira Ranges. During the Chewings Orogeny the c.1790 Ma D_1 structures were transposed into a composite S_1/S_2 fabric. Map scale F_2 folding is interpreted to have a shallow plunge suggesting that the S_1 fabric may have originally been shallow dipping, raising the possibility that deformation was extensional in nature, and coeval with deposition of the nearby Reynolds Range Group which is constrained to the interval 1806-1785 Ma. Although inferred here to be Yambah aged, the timing constraints for D_1 /M_1 also overlap with the c. 1800 Ma Stafford Event which was associated with voluminous felsic magmatism, mafic magmatism and extreme geothermal gradient magmatism. This suggests that an extended period of extension, sedimentation, magmatism and deformation may have occurred at around 1800 Ma in the central Aileron Province.

KEYWORDS

Yambah, Chewings, Geochronology, Boothby, central Australia, Proterozoic, Tectonic, Deformation, Geochronological.

TABLE OF CONTENTS

LIST OF FIGURES AND TABLES

INTRODUCTION

The assembly or growth of the Australian continent during the Paleoproterozoic (c. 1950-1600 Ma) period has been proposed to have occurred as a consequence of collisional accretion processes related to north directed subduction beneath the North Australian Craton (Scrimgeour *et al.* 2005, Betts & Giles 2006, Wade *et al.* 2006, Cawood & Korsch 2008). During this period, the North Australian Craton (Figure 1) was generally characterised by high-geothermal gradient metamorphism punctuated by basin development and extensive magmatism that affected the southern part of the North Australian Craton. Table 1 summarises the history of tectonic events during the Paleoproterozoic period.

Contrasting with the generally high geothermal gradient tectonism in the North Australian Craton, high pressure deformation has been identified within the Yaya Metamorphic Complex in the Warumpi Province (Scrimgeour *et al.* 2005). The high pressure metamorphism is interpreted to record the suturing between the southern margin of the North Australian Craton and the Warumpi Province (Scrimgeour *et al.* 2005, Selway *et al.* 2009). This event has been termed the Liebig Orogeny (Scrimgeour *et al.* 2005). The date for collision is estimated at ca. 1640 Ma based on metamorphic zircon growth from a high pressure granulite (Scrimgeour *et al.* 2005).

Further west in Western Australia, 1780 Ma tectonism is also interpreted to have been associated with high pressures(Smithies & Bagas 1996). At about this time, granitoids known as the CAT suite (Zhao & McCulloch 1995, Giles *et al.* 2002) intruded into the southern part of the North Australian Craton and are proposed to provide evidence of subduction along the south eastern margin of the Arunta region (Foden *et al.* 1988, Giles *et al.* 2002, Maidment *et al.* 2005, Betts & Giles 2006).

Table 1 History of major tectonic events during the Paleoproterozoic period in the North Australian Craton.

Tectonic Event	Age (Ma)	Description
Stafford Event	1880-1820	High temperature, low pressure, regional greenschist to granulite facies metamorphism (Collins & Shaw 1995, White *et al.* 2003). Metamorphism and deformation spatially related to intrusion of Mt Stafford and Harveson granites (c. 1818 Ma; Hand and Buick, 2001). No pervasive deformation, described as regional contact metamorphism (Hand & Buick 2001). Mafic magmatism. Interpreted as an extensional tectonic event (Claoué-Long & Hoatson 2005).
Yambah Event	1790-1770	High temperature, low pressure, regional granulite metamorphism in the northern Aileron region coeval with a large amount of syntectonic granitic magmatism. Minor pre-, syn- and late granitic magmatism in the central Aileron region(Collins & Shaw 1995). Mafic magmatism. Interpreted as an extensional tectonic event (Claoué-Long & Hoatson 2005).
Inkamulla Igneous Event	1760-1740	Granitic and mafic magmatism in the Southeastern Aileron region including apparent A-type and arc related magmatism. Deformational and metamorphic character unknown (Scrimgeour *et al.* 2005).
Strangways Event	1740-1690	High temperature, medium pressure granulite metamorphism. Pervasive deformation with kilometer-scale sheath folds related to NE-SW overthrusting (Collins & Shaw 1995, Claoué-Long *et al.* 2008a, Claoué-Long *et al.* 2008b). Crustal thickening. Interpreted as a compressional tectonic event. Late dolerite dyke swarm indicates the end of the event may have been extensional (Claoué-Long & Hoatson 2005, Claoué-Long *et al.* 2008b)
Argilke Igneous Event	1690-1670	Volumetrically significant predominantly felsic magmatism. Metamorphic character poorly understood but up to amphibolites grade. Deformational character unknown (Scrimgeour *et al.* 2005)
Liebig Orogeny	c. 1635	High temperature, high pressure metamorphism in the Yaya Metamorphic Complex in the Warumpi province(Scrimgeour *et al.* 2005). Interpreted as recording the accretion of the exotic Warumpi Province to the North Australian Craton(Scrimgeour *et al.* 2005, Wade *et al.* 2006). Voluminous granite and charnokite intrusions. Coeval mafic and ultramafic magmatism suggest that the Liebig Orogeny was at some point part of an extensional tectonic setting (Claoué-Long & Hoatson 2005)
Chewings Orogeny	1600 – 1540	High temperature, medium pressure metamorphism from greenschist to upper granulite facies. Metamorphic grade increases from west to east in the Reynolds Range region (Dirks *et al.* 1991, Collins & Shaw 1995, Hand & Buick 2001)

These accreationary/collisional style process are envisaged to have resulted in continental growth through the addition of comparatively juvenile magmas into the North Australian Craton, as well as the incorporation of continental ribbons also composed of comparatively juvenile rocks (Scrimgeour *et al.* 2005). The evidential record of juvenile magmatic additions is still poorly documented however.

An alternative model for the formation of continental crust, proposed by Collins (2002a, b), is via basin infill in extensional back arc regions above subducting oceanic lithosphere with intermittent compressional phases induced by the flat subduction of buoyant oceanic plateaus. In this model the overall tectonic history is largely an extensional one characterised by high geothermal gradients and extensive magmatism which is largely derived by the thermal reworking of basinal packages and the extended continental crust they were deposited on.

In Proterozoic Central Australia the possibility of an extended extensional tectonic regime is supported by the presence of mafic and ultramafic intrusions which are coeval with most of the major tectonic cycles (Claoué-Long & Hoatson 2005) listed in Table 1. Furthermore, Claoué and Hoatson (2005) propose that mafic intrusions in the Stafford Event and Yambah Events show chemical characteristics indicative of an extensional back-arc continental margin setting between 1810-1770 Ma (Claoué-Long & Hoatson 2005). The prescence of dolerite dykes coeval with the end of the Strangways Event (c. 1690 Ma; Claoué-Long & Hoatson, 2005) may also indicate an extensional environment (Claoué-Long & Hoatson 2005). Additionally mafic to ultramafic magmatism in the southern Aileron Province at 1640 Ma, at the same time as proposed collision during the Liebig Event (Scrimgeour *et al.* 2005), suggests that an extensional regime may have also operated at some time during this period (Claoué-Long & Hoatson 2005).

The generally high-geothermal gradient events (Dirks *et al.* 1991, Collins & Shaw 1995), a southward migrating spatially organised pattern of basin development (Giles *et al.* 2002, Betts & Giles 2006) with associated mafic magmatism followed by granitic magmatism and high geothermal metamorphism, is more easily reconciled with extensional continental formation.

In this project the timing of magmatic events in the Mt Boothby region in the eastern Reynolds Range will be investigated. The Mt Boothby region occupies a critical location in the southern part of the North Australian Craton. To the north is the extensive system of metasedimentary and magmatic rocks that appear to predominantly record events that are older than c. 1800 Ma (Claoué-Long *et al.* 2008a). To the south-east are regions that record interpreted 1780-1760 Ma arc-related magmatism (Zhao & McCulloch 1995, Giles *et al.* 2002) and the later high temperature 1730-1690 Ma Strangways Event and 1640 Ma Liebig Orogeny (Giles *et al.* 2002, Claoué-Long & Hoatson 2005, Cawood & Korsch 2008, Claoué-Long *et al.* 2008b). Therefore the Mt Boothby area occupies a linking position between the older events to the north and the younger ones to the south-east. In an attempt to better understand the timing of tectonic events in the southern part of the Aileron Province this project will aim to determine the timing of magmatism, high grade deformation and associated *P-T* conditions in the Mt Boothby region. Of particular focus is a deformed composite mafic gneiss unit. The mafic nature of this rock combined with its relative deformational complexity to adjacent intrusive rocks and its location within the wider Arunta region suggest it may form a key lithology for constraining crustal deformation and growth events.

The specific aims of the project are to map structural relationships in the Mt Boothby region which will then be coupled with U-Pb zicon and monazite geochronology to

determine the timing of magmatism and high grade metamorphism. Combined with pressure and temperature constraints on metamorphism this information will allow us to construct a tectonostratigraphic model for the region and test the hypothesis that the composite mafic-felsic gneiss records paleoproterozoic, ~ c. 1800 Ma, deformation within a high geothermal gradient, extensional, tectonic setting.

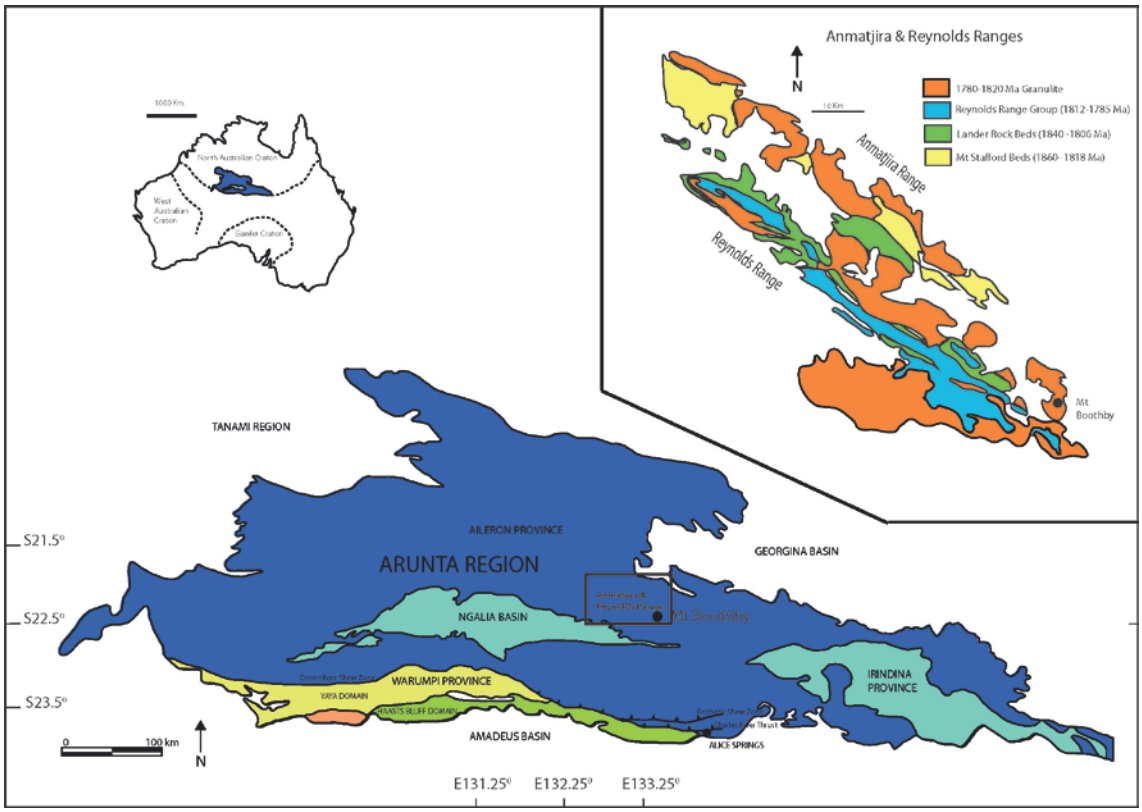

Figure 1 Locality map showing the Arunta region within the North Australian Craton and the location of Mt Boothby within the south eastern Reynolds Range.

GEOLOGICAL SETTING

The Arunta Complex in Central Australia is a large (~200,000 km²) polydeformed and metamorphosed terrane (Collins & Shaw 1995, Hand & Buick 2001, Claoué-Long *et al.* 2008a) which is divided into the predominantly Paleoproterozoic Aileron, Warumpi and Irindina Provinces (Teyssier *et al.* 1988, Claoué-Long *et al.* 2008a).

Mt Boothby is located near the south eastern end of the 70 km long Reynolds Range within the Aileron Province of the Arunta Complex (Figure 1). The oldest exposed rocks in the Reynolds Range region are the Lander Package that are a sedimentary sequence deposited between 1840 and 1806 Ma (Vry *et al.* 1996, Hand & Buick 2001). The Lander Package represent more than 60% of the exposed geology in the Arunta region (Claoué-Long & Hoatson 2005). This sequence consists of metamorphosed mudstones, siltstones and sandstones (Hand & Buick 2001). Early granitic rocks, such as the Harverson Granite (c. 1818 Ma) and Yaningigjara Orthogneiss (c. 1806 Ma; Hand & Buick 2001), intrude the Lander Package and combined, these rocks form a basement for the younger Reynolds Range Group (1812-1785 Ma; Vry *et al.* 1996, Hand & Buick 2001). The Reynolds Range Group consists of metamorphosed sandstone, mudstone, marl and limestone. The group was extensively intruded by megacrystic granitic rocks such as the Napperby Gneiss, at ~ 1780 Ma (Hand & Buick 2001).

The Chewings Orogeny (ca. 1600 Ma) is the most pervasive metamorphic event in the Reynolds Range and is evident in both the Lander Package and Reynolds Range Group (Vry *et al.* 1996, Williams *et al.* 1996, Hand & Buick 2001, Rubatto *et al.* 2001). The metamorphic grade evident from this low pressure phase increases from the northwest to southeast along the Reynolds Range region with low grade greenschist facies (~400 °C) to granulite facies (~750-800 °C) in the Mt Boothby region (Hand & Buick 2001).

Geology of the Mt Boothby area

Structural and lithologic field mapping and sample collection was carried out in the Mt Boothby region to provide a framework for geochronological interpretation. The primary focus of mapping was on structural fabrics within a polydeformed composite mafic-felsic gneiss and the surrounding rocks with which it is in contact. The lithologies in the area consist of the aforementioned mafic-felsic gneiss, metasedimentary lithologies and the Mt Boothby Orthogneiss.

METASEDIMENTS

Metasedimentary lithologies are migmatitic and generally have cordierite-sillimanite – K-feldspar-quartz-biotite assemblages. The primary lithologic layering is evident in places through compositional variations in quartz rich to more metapelitic layers which in places show a transition suggesting the presence of recrystallised graded beds. The foliation is defined by sillimanite and biotite which parallels primary lithological layering and stromatic leucosome segregations consist of quartz-K-feldspar ± cordierite. Where retrograde shear zones (Raimondo *et al.* 2011) overprint the metasediments the shear fabric is defined by muscovite and biotite and may contain relic K-feldspar. In some instances segregations up to 30cm long and 10cm wide consisting of cordierite, K-feldspar and minor quartz cross cut the fabric. Locally, pegmatites up to 1m wide and 10-15m long cut the layering in the metapelites.

COMPOSITE MAFIC-FELSIC GNEISS

The composite mafic-felsic gneiss is located to the north, north east and west of the summit of Mt Boothby (Figure 2). The rock is a polydeformed migmatitic gneiss with

compositional mafic and felsic interlayering defining the foliation. The mineral assemblage is orthopyroxene-clinopyroxene-hornblende-plagioclase-K-feldspar and quartz with the mafic and felsic layers being defined by variations in modal proportions of mafic minerals. The scale of the compositional layering is below map scale however in the vicinity of grid reference 032530E 750220N the lithology is particularly mafic rich and is mapped as a meta-gabbro unit. Leucosomal segregations for the most part are layer parallel but locally form small veins that cross cut the foliation within discrete shear bands.

MT BOOTHBY ORTHOGNEISS

The Mt Boothby Orthogneiss bounds the composite mafic-felsic on the western and northern sides (Figure 2). The mineral assemblage is biotite-K-feldspar-plagioclase and quartz. K-spar augen are present throughout the rock ranging up to approximately 8cm in length but generally 2-3 cm. Biotite defines the foliation in the rock. The orthogneiss is locally migmatitic with interpreted partial melts forming discordant veins and patches. At the contact with the composite mafic-felsic gneiss a complex mingled zone of composite mafic-felsic and Mt Boothby Orthogneiss occupies a domain ranging from approximately 20-100 m wide on the NE boundary between the two lithologies. In this area large migmatitic melt veins are present cross cutting the foliation. The orthogneiss contains rare xenoliths of cordierite-rich granofels which are interpreted to have been derived from the adjacent metasediments.

MICROGRANITE

Rare small bodies of microgranite that form narrow dykes up to 80 cm across and 15m long occur within the composite mafic-felsic gneiss. These are unfoliated and have

'mingled' margins within the enclosing rocks. Where the boundaries are discrete the microgranites clearly truncate the layering suggesting they are late in the deformational history.

STRUCTURAL EVOLUTION

The generalised structural geology is shown in Figure 2. The oldest readily identifiable structural fabrics in the mapped area occur in the composite mafic-felsic gneiss. This unit contains abundant evidence for a transposed fabric, with > 30% of outcrops containing isoclinal F_2 folds. The S_1 form surface to the folds is defined by the mafic-felsic compositional layering, migmatitic segregations and aligned hornblende and pyroxene. Overall the foliation in the composite mafic-felsic gneiss is designated as a composite S_1/S_2 fabric, although not all outcrops show evidence of fabric transposition and it is possible that some components of the mafic-felsic association have not experienced a polydeformational history. The composite S_1/S_2 fabric trends ~ NNE with F_2 folds plunging NE or SW but with widely varying angles ranging from 0°- 79°. In many instances it is hard to determine plunge because of the tight fold profiles and the rounded nature of the outcrop. However, based on vergence relationships of mesoscale F_2 folds in the composite mafic-felsic gneiss a map-scale synformal structure is interpreted to trend approximately NE-SW through the composite mafic-felsic unit (Figure 2). The overall plunge of this structure is not known, however the composite mafic-felsic unit continues at least 1 km to the east, and can also be traced ~ 2 km to the west. This suggests that at map scale the plunge may be shallower than the predominately steeply plunging meso-scale F_2 folds.

In contrast to the mafic-feslic gneiss association, the adjacent metasediments show no obvious fabric transposition, and contain an apparently simple gneissic foliation defined

by aligned sillimanite-biotite and quartz-feldspathic segregations that parallel original compositional layering. However outside the mapped area to the north at around grid reference 0325624E 7504474N, metasedimentary rocks do show evidence of polydeformation with an early gneissic fabric (S_1) defined by aligned sillimanite-biotite and quartz-feldspathic segregations outlining mesoscale isoclinal folds that contain S_2 sillimanite-biotite axial plane fabrics. However the bulk of the metapelites only show a simple foliation, and potentially the intensity of D_2 in these units has largely obliterated the D_1 structures.

In contrast to the polydeformation evident in the mafic-felsic gneiss and some of the metasedimentary lithologies in the area, the structural fabric in the Mt Boothby Orthogneiss appears to have a less complex character. Overall the original granitic character of the orthogneiss is still easily discernible suggesting that strain has not obliterated earlier structural fabrics in this unit. The main structural fabric is designated S_2 on the basis that the granitic protolith to the orthogneiss locally truncates the gneissic fabric in the composite mafic-felsic gneiss (Figure 3a), while the orthogneiss fabric is parallel to the overall composite S_1/S_2 fabric in the mafic-felsic gneiss. An exception to this simple structural picture in granitic orthogneiss occurs outside the mapped area to the north at grid reference 0324830E 7505997N, where a migmatitic orthogneiss contains a transposed fabric S_1/S_2 fabric. However in this case, the orthogneiss is intensely layered.

The presently moderate to steeply dipping S_2 and composite S_1/S_2 fabrics are locally reoriented by D_3 structures that form open warp-like features that range in scale up to 10m wide, by are mostly 1-2m in scale. These dominantly occur in the orthogneiss, the most obvious of which is a 100m-scale east trending kink like fold that reorients S_2 into

a shallow-dipping position at grid reference 0325200E 7502700N. On the mesoscale F_3 structures are associated with minor migmatisation.

F_3 and the earlier structures are overprinted by two styles of shear zone; comparatively anhydrous mylonites and hydrous schist zones. The anhydrous mylonites occur within the metaigneous lithologies. They are generally steeply dipping and trend NE-SW, and are up to 50m wide and can be traced for up to 1km. Shear sense indicators in the mylonites show dextral movement.

Hydrous shear zones occur in both the metasediments and metaigneous lithologies. The foliation is defined by muscovite and biotite and generally trends NW-SE. The shear zones are up to 20m wide and can be traced for up to 300m. Shear sense is dextral. The relationship between the two style of shear zones is not definitive, although in some instances muscovite-bearing alteration overprints the mylonites suggesting that the hydrous shear zones may be younger.

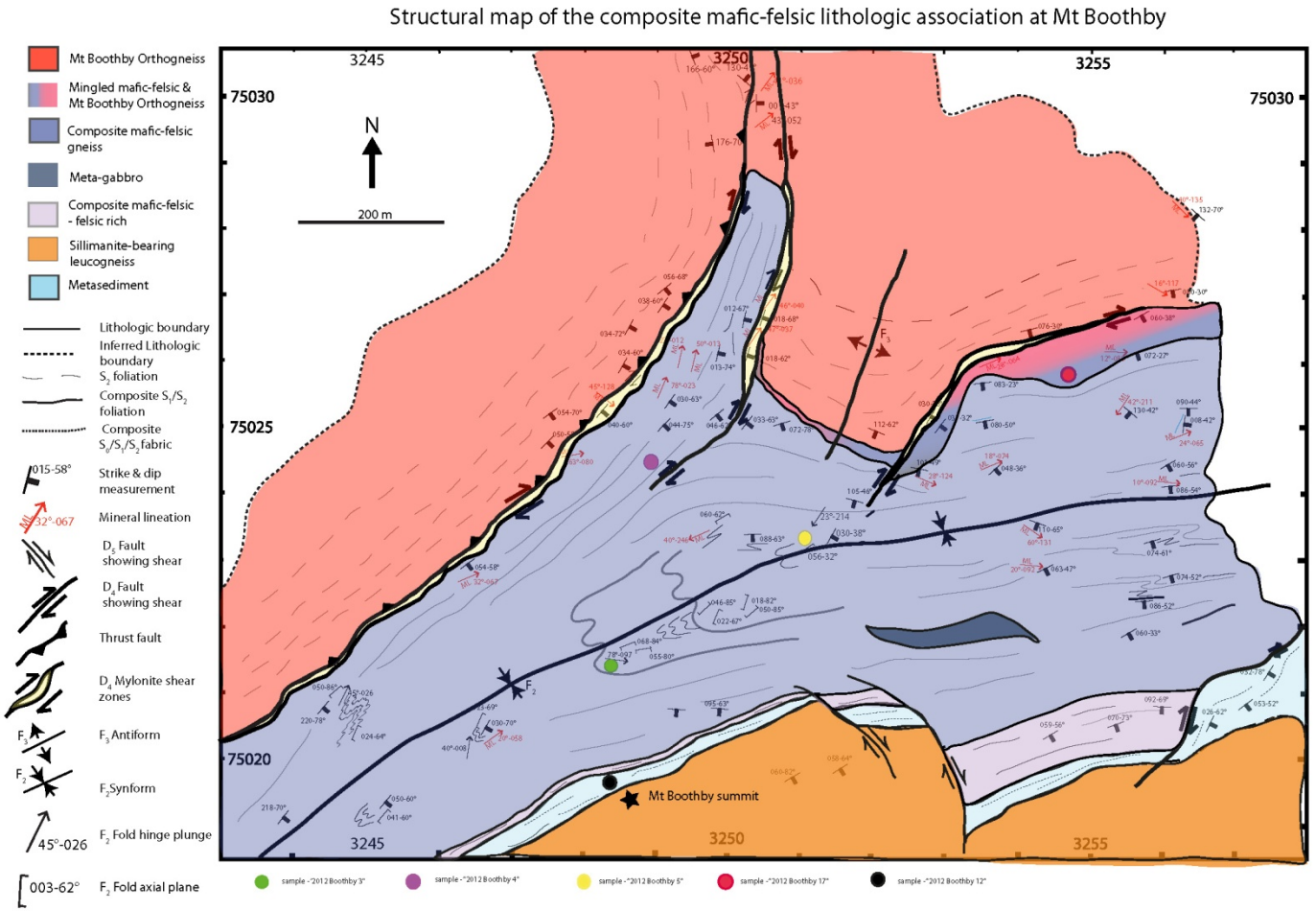

Figure 2 Structural map of the composite mafic-felsic at Mt Boothby with sample locations.

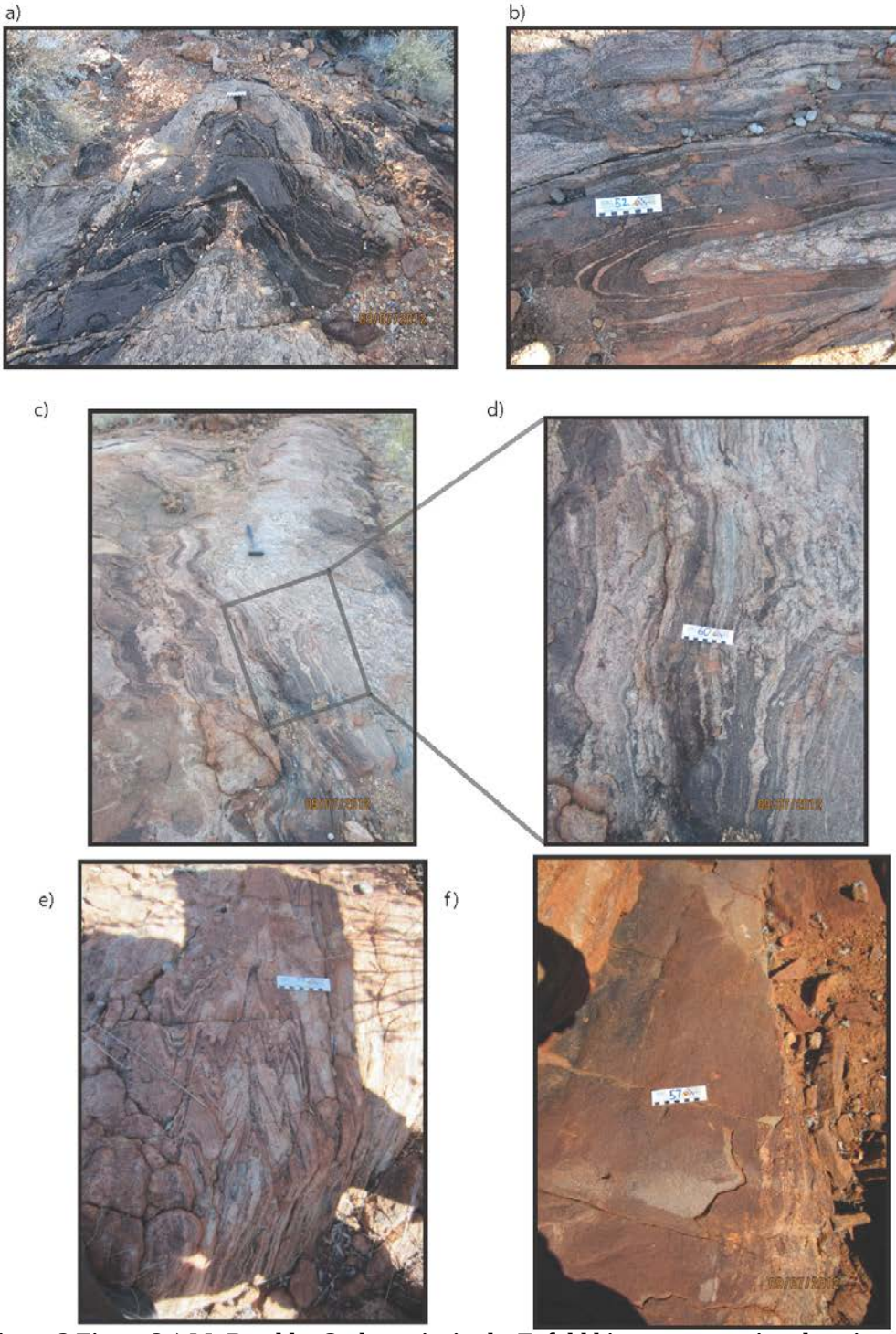

Figure 3 Figure 3a) Mt Boothby Orthogneiss in the F_2 fold hinge cross cutting the migmatitic S_1 fabric in the composite mafic-felsic gneiss. The sample *2012 Boothby 17* was taken from this outcrop. b) Isoclinally folded composite mafic-felsic with Mt Boothby Orthogneiss in the F_2 hinge. c) Outcrop of mingled composite mafic-felsic gneiss and Mt Boothby Orthogneiss showing the complex deformation and intrusive relationship of the two lithologies. d) A close up from c) showing the mingling lithologies. e) F_2 M-folds in the composite mafic-felsic gneiss which define the hinge zone of a regional scale F_2 fold. f) Unfoliated micro-granitic dyke, '2012 Boothby 14'.

METHODS

Geochronology

The monazite and zircon was separated before images of the grains were captured using Back Scatter Electron imaging for the monazites and Cathode Luminescence imaging for the zircons (see Appendix C for a detailed methodology).

U-Pb isotopic analysis used a New Wave 213nm Nd-YAG laser in a He ablation atmosphere, coupled to an Agilent 7500cs ICP-MS. For the monazites, a 50 s gas blank was analysed followed by 50 s of measurement during ablation. For the zircons, a 40 s gas blank was followed by an 80 s ablation analysis. The beam diameter at the sample surface was 15 um for monazite ablation with 30 um used for zircon ablation. Isotopes measured on the monazites were ^{204}Pb, ^{206}Pb, ^{207}Pb, and ^{238}U with 10, 15, 30 and 15 ms dwell times respectively whilst for the zircons ^{208}Pb and ^{232}Th were also measured each with 10 ms dwell times. ^{238}U was calculated using a ^{238}U/^{235}U ratio of 137.88. ^{204}Pb was monitored to assess potential influence on sample analysis but was not used for a common-Pb correction due to an interference of ^{204}Hg on this mass (Payne *et al.* 2006, Payne *et al.* 2008, Payne *et al.* 2010).

Zircon and monazite age calculations were made using Glitter software version 4.0 (Jackson *et al* 2004, Griffin *et al.* 2008). U-Pb fractionation was corrected using the MAdel standard for monazites and the GEMOC GJ-1 standard for zircons. Precise TIMS data for the MAdel standard gives two distinct ages 4 Ma apart, however these are within uncertainty for the LA-ICPMS method and therefore are not considered in age calculations (Payne *et al.* 2006, Payne *et al.* 2008, Payne *et al.* 2010). Age data accuracy was confirmed by analysis and comparison of in house standards, the 94-

222/Bruna-NW monazite standard, ca 450 Ma (Maidment 2005), and Plesovice zircon standard, 337.13±0.37 Ma (Sláma *et al.* 2008).

Throughout the study, the weighted averages obtained for GJ are $^{207}Pb/^{206}Pb$= 608.9±3.7 Ma (*n*=257, MSWD=0.46), $^{206}Pb/^{238}U$= 601.0 ± 1.3 Ma (*n*=257, MSWD=2) and $^{207}Pb/^{235}Pb$= 602.6 ±1.1 Ma (*n*=257, MSWD=1.6) and Plešovice are $^{207}Pb/^{206}Pb$= 343.8 ± 6.7 Ma (*n*=79, MSWD=0.59), $^{206}Pb/^{238}U$= 335.6 ± 2 Ma (*n*=79, MSWD=4.5) and $^{207}Pb/^{235}Pb$= 336.6 ± 1.8 Ma (*n*=79, MSWD=3.6).

Throughout the study, the weighted averages obtained for MAdel are $^{207}Pb/^{206}Pb$= 499.1±11 Ma (*n*=68, MSWD=2.6), $^{206}Pb/^{238}U$= 519.6±2.4 Ma (*n*=68, MSWD=1.6) and $^{207}Pb/^{235}Pb$= 515.6±2.9 Ma (*n*=68, MSWD=3.1), 222 are $^{207}Pb/^{206}Pb$= 463±10 Ma (*n*=27, MSWD=0.85), $^{206}Pb/^{238}U$= 451.4±5 Ma (*n*=27, MSWD=3.5) and $^{207}Pb/^{235}Pb$= 450.9±3.5 Ma (*n*=27, MSWD=2.1).

Reduced monazite and zircon data was then exported into excel where subsequent conventional concordia and weighted average plots were generated using Isoplot v4.11(Ludwig 2003). Ages quoted throughout the study are $^{207}Pb/^{206}Pb$ ages as the data contains ages older than *c.* 1000 Ma and all errors stated in data tables and alongside concordia diagrams are at the 1σ level The error on the overall age of each sample is given at the 2σ level. Concordancy was calculated using the ratio of ($^{206}Pb/^{238}U$) / ($^{207}Pb/^{206}Pb$).

GEOCHRONOLOGY RESULTS

The U-Pb ages and sample grid references are summarised in Table 2, and Figures 6-15. The complete data tables are contained in Appendix A. The sample locations are shown in Figure 3 when within the map area and Figure 5 for two samples outside the

map area. In general, for all weighted average calculations analyses used are within 5% of concordant and are not reversely concordant by more than the error margin, shown as an error elipse on the concordia plots.

Table 2 A summary of all geochronology results obtained in this study

Sample			Description	Location
Igneous Rock	***Magmatic Age***	**Metamorphic Age**		
2012 Boothby 3 – mafic	1773±6.4 Ma – Zircon. Late magmatic phase		Composite mafic-felsic gneiss (mafic) – low strain zone	53K 0323472E 7502013N
2012 Boothby 3 – felsic	1772±10 Ma – Zircon. Late magmatic phase		Composite mafic-felsic gneiss (felsic) – low strain zone	53K 0323472E 7502013N
2012 Boothby 4		1789±13 Ma – Zircon. Early D_1 metamorphism.	Composite mafic-felsic. High strain zone	53K 0324842E 7502465N
2012 Boothby 5		1796±12 Ma – Zircon. Early D_1 metamorphism.	Composite mafic-felsic. Low strain zone	53K 0325114E 7502342N
2012 Boothby 17	1788±15 Ma - Zircon	1553±10 Ma - Monazite	Megacrystic orthogneiss	53 K 0324817E 7502155N
MB0818	1795±8.5 Ma - Zircon	1534±10 Ma - Monazite	Megacrystic orthogneiss	53K 0324830E 7505997N
2012 Boothby 14	1573±15 Ma - Zircon	1523±28 Ma - Monazite	Micro Granite	53K 0324844E 7502119N
Metasediments	**Detrital – Max Deposition**			
2012 Boothby 12	1830 Ma	1549±10 Ma - Monazite	Metasedimentary Gneiss	53K 0324924E 7502080N
Boothby OSM	1858 Ma	1551±9 Ma - Monazite	Metasedimentary Gneiss	53K 324708E 7506172N

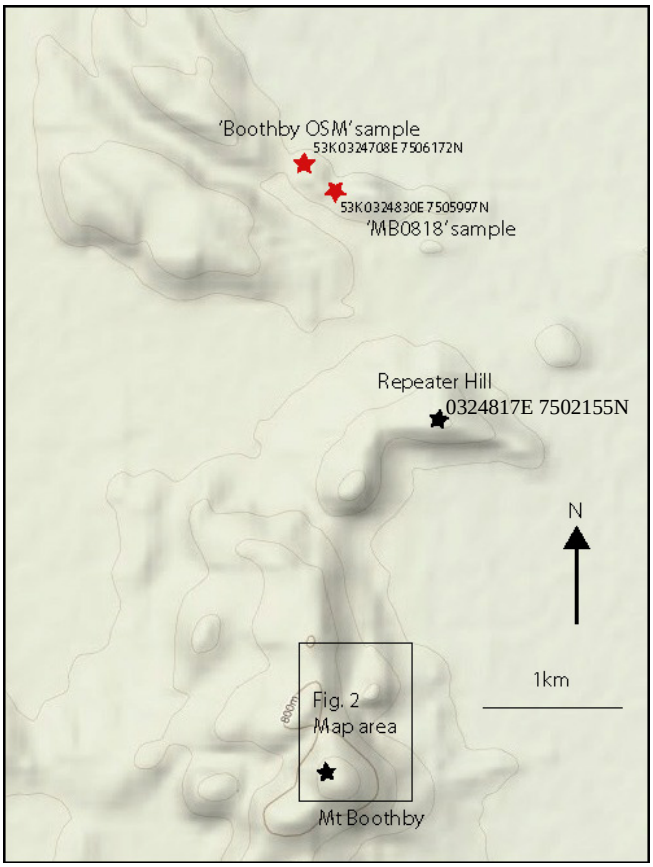

Figure 4 Map showing the locations of the two samples collected from outside of the map area along with their grid reference. The map area is highlighted to the south and the location 'Repeater Hill' with grid reference show the location of the isoclinally folded metasediments.

U-Pb zircon geochronology

COMPOSITE MAFIC-FELSIC GNEISS

The composite mafic-felsic gneiss is a hornblende-biotite-orthopyroxene-plagioclase-K-feldspar gneiss (petrographic photo Appendix B) that has compositional mafic and felsic domains. Based on both the homogeneity of the mafic-felsic gneiss at map-scale and the mineral assemblage, the sample is interpreted to have an igneous protolith. Three samples were analysed from this lithological association. They were samples *2012 Boothby 3*, *2012 Boothby 4* and *2012 Boothby 5*. In *2012 Boothby 3* the mafic and felsic components were analysed separately.

Sample - 2012 Boothby 3 – mafic

Zircons from sample *2012 Boothby 3 – mafic* are generally euhedral and often elongate with average aspect ratios of 3:1 (Figure 5). The zircons range between 80–200 μm in size with shorter, more rounded, zircons with an aspect ratios ranging from to 2:1 to 4:1. The cores generally consist of large oscillatory zoned areas, often occupying most of the zircon, that are lighter in colour than surrounding zones or rims. Some grains also have a second core, internal to the oscillatory zoned cores, which are dark and homogenous or have only subtle oscillatory zoning. Further dark coloured zoned overgrowths and rims are present on the grains ranging from <5 μm up to 30 μm wide.

Fifty-seven of zircon analyses targeted cores and oscillatory zoned domains giving a weighted average $^{207}Pb/^{206}Pb$ age of 1773.2±6.4 Ma (MSWD = 0.55) from 42 analyses and an upper intercept age of 1773.3±5 Ma (MSWD = 4.9) from 57 analyses. The weighted average age is adopted as the age of this zircon population and the igneous protolith. Ten analyses targeted rims and a weighted average from 5 of these analyses give a $^{207}Pb/^{206}Pb$ age of 1759±18 Ma (MSWD = 1.2) although this age is of limited use due to the small number of analyses.

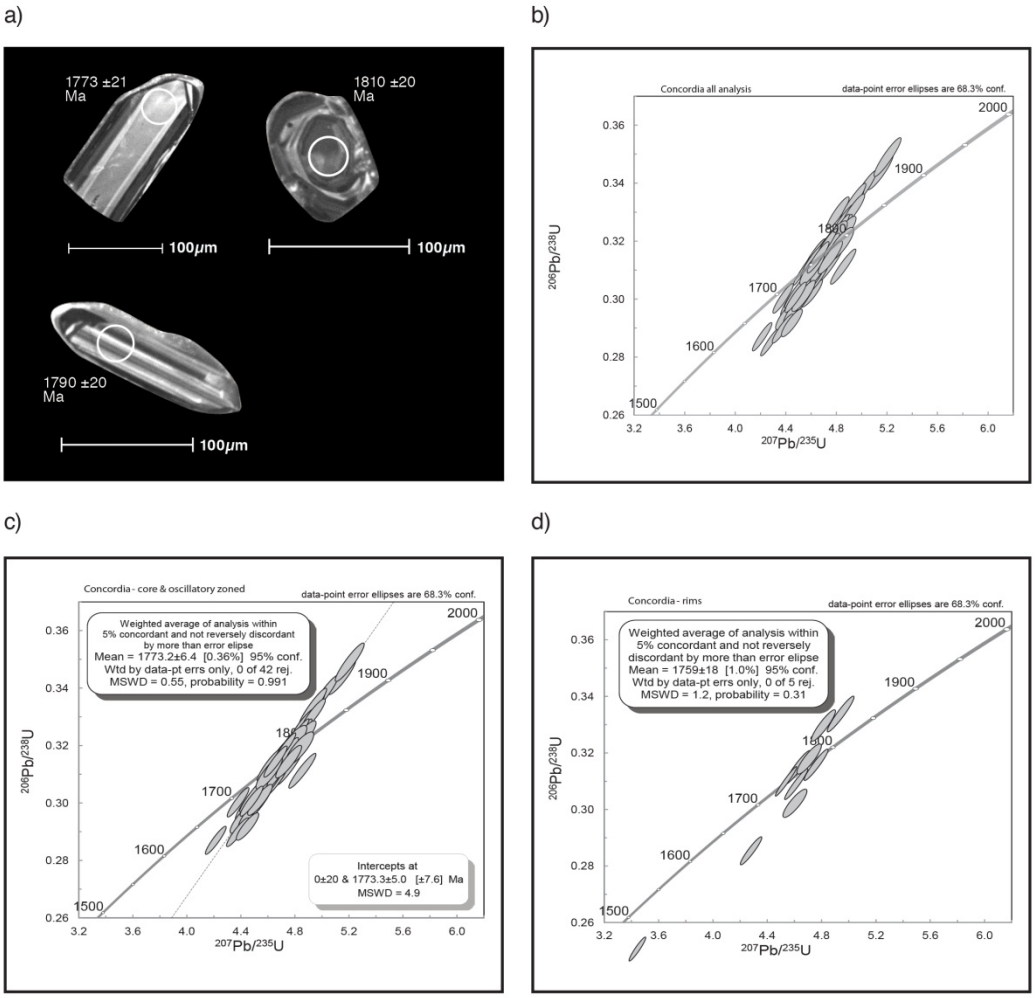

Figure 5 Sample *2012 Boothby 3 – mafic* a) Example of CL images of zircon grains. White circles show positions targeted on LA-ICP-MS with ^{207}Pb /^{206}Pb isotope ages shown. b) Concordia plot of all zircon grains sampled. c) Concordia plot of only core & oscillatory zones showing an intercept age and a ^{207}Pb /^{206}Pb isotope weighted average age in insets.

Sample - 2012 Boothby 3 – felsic

External zircon morphologies and internal CL features are similar to those seen in *2012 Boothby 3 – mafic*. However more zircon grains show dark homogeneous to irregular diffuse cores (Figure 6).

Thirty seven zircon analyses targeted cores or regions of oscillatory zonation. Twenty-three of these analyses give a weighted average ^{207}Pb/^{206}Pb age of 1772±10 Ma (MSWD = 1.14) and all thirty-seven analyses give an upper intercept age of 1768±11 Ma

(MSWD = 10.6). Again, the weighted average age is used as most analyses are near concordant.

Only four rims were able to be targeted. Two were reversely discordant by larger than the error ellipse, analysis '38R' & '39R', which gave $^{207}Pb/^{206}Pb$ ages of 1569 ± 22 Ma and 1575 ± 24 Ma. The remaining ages were, 1765.1 ± 22 Ma from analysis '2R' which was 92% concordant, and 1783.2 ± 20 Ma from analysis '27R' which was 95% concordant.

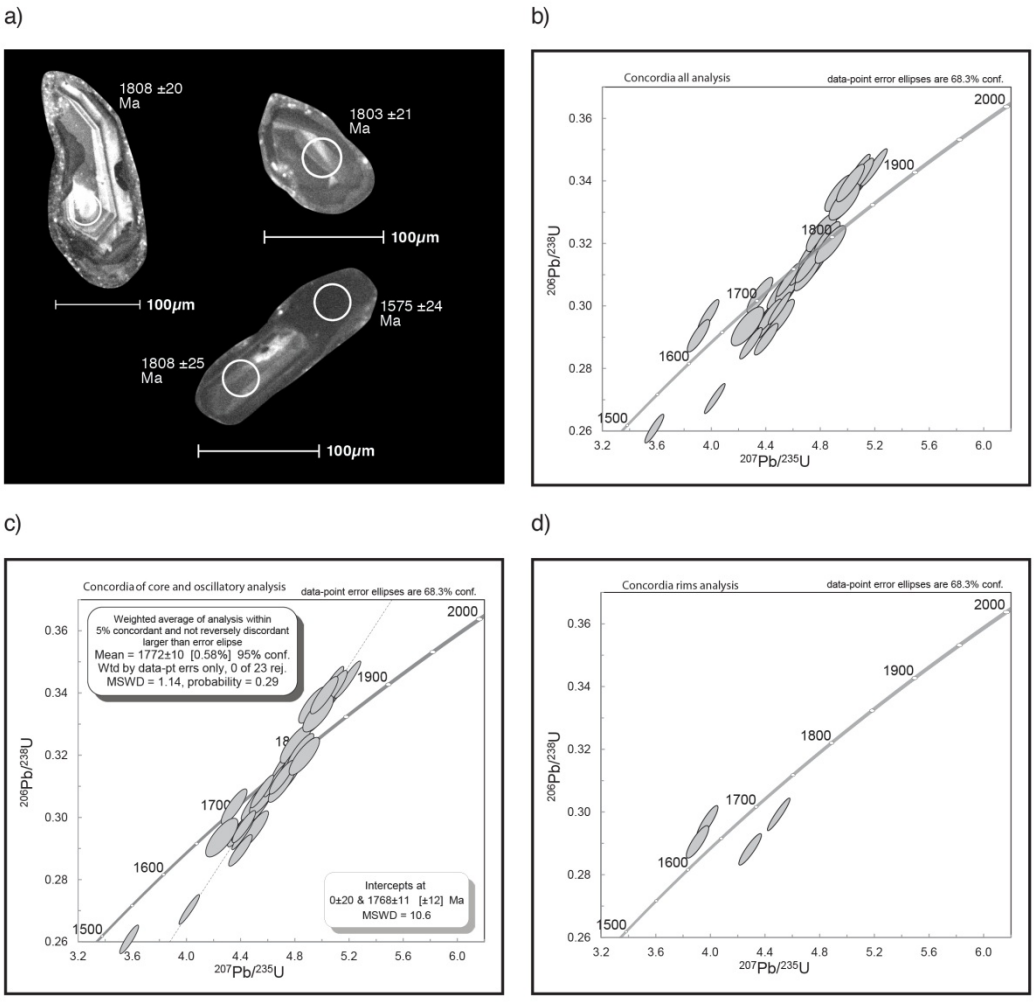

Figure 6 Sample *2012 Boothby 3 – felsic* a) Sample CL images of zircons. White circles show positions targeted on LA-ICP-MS with $^{207}Pb/^{206}Pb$ isotope ages shown. b) Concordia plot of all zircon grains sampled. c) Concordia plot of only core & oscillatory zones showing a weighted average and a concordia intercept age. d) Concordia of rim analyses.

Sample - 2012 Boothby 4

2012 Boothby 4 was sampled from an inferred D_2 high strain zone on the interpreted limb of a regional scale NE-SW trending F_2 fold (Figure 2) and was chosen as a comparative sample to the samples from the low strain hinge zone (*2012 Boothby 3* and *2012 Boothby 5*).

Zircon morphology is dominated by euhedral-subhedral grains with aspect ratios ranging from 2:1 to 3:1 and sizes between 80 – 180 um (Figure 7). Under CL the majority of the grains are dark and homogeneous but occasionally show some subtle oscillatory zoning. Two zircons contain bright cores which are probably inherited grains (Corfu *et al.* 2003, Hoskin & Schaltegger 2003).Thirty-two analyses were done on the dark zones of the zircon grains. A weighted average age of 1789±13 Ma (MSWD = 1.19) and an upper intercept age of 1786±20 Ma (MSWD = 15) is calculated from seventeen and twenty-nine analyses respectively. The weighted average age of 1789 ± 13 Ma is the preferred age.

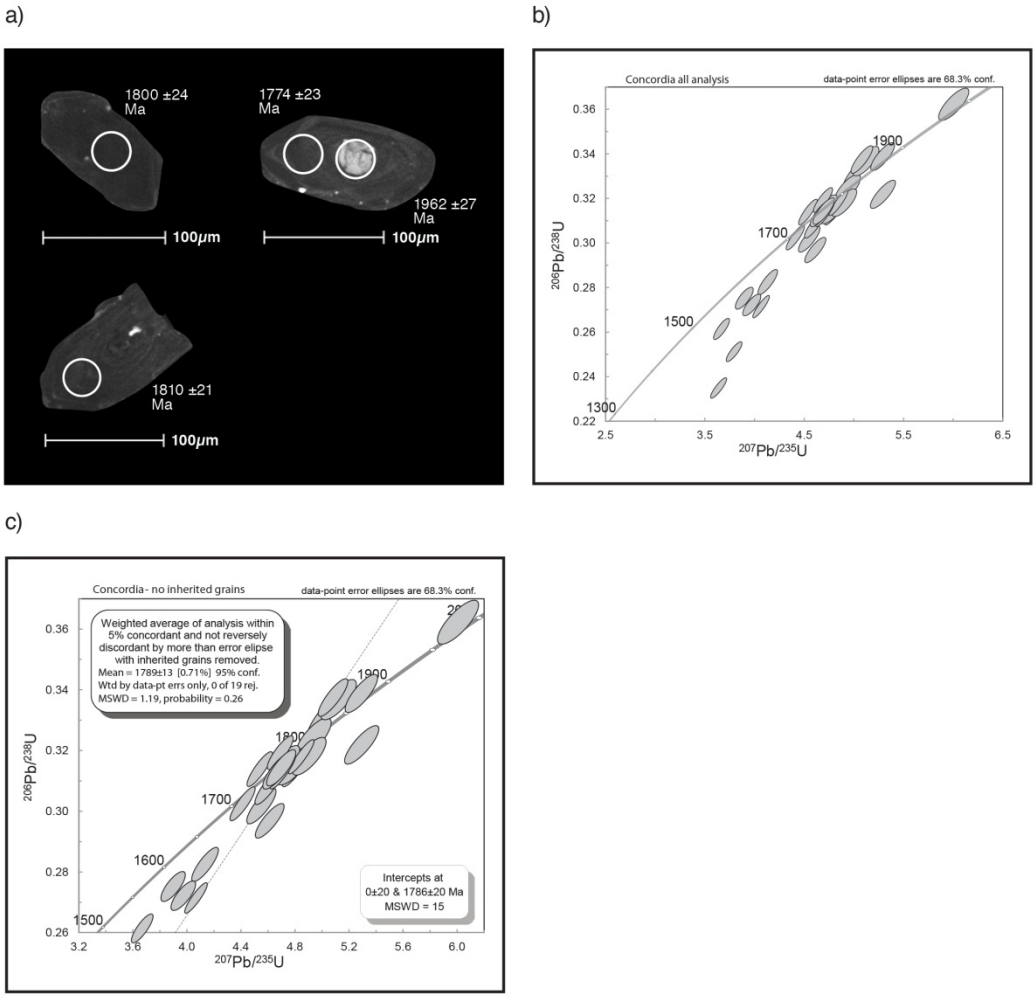

Figure 7 Sample *2012 Boothby 4*. a) Example of CL images with white circles showing positions targeted on LA-ICP-MS with $^{207}Pb/^{206}Pb$ isotope ages shown. b) Concordia plot of all analyses. c) Concordia plot with no inherited grains. Upper inset shows a weighted average age.

Sample - 2012 Boothby 5

This sample is from an interpreted low strain hinge zone of the interpreted regional F_2 fold (Figure 2). Zircon grains are subhedral, generally dark and homogeneous or show irregular and diffuse zoning with some subtle oscillatory zoning apparent in some grains. The zircons are 50 – 150 μm (Figure 8) with aspect ratios of 2:1 to 3:1. Twenty five analyses were done on cores and oscillatory zoned domains. A weighted average age of 1796±12 Ma (MSWD = 0.76) and an upper intercept age of 1780±13 Ma

(MSWD = 10.3) were calculated from thirteen and twenty-five samples respectively. Two analyses that targeted rims were both more than 5% discordant.

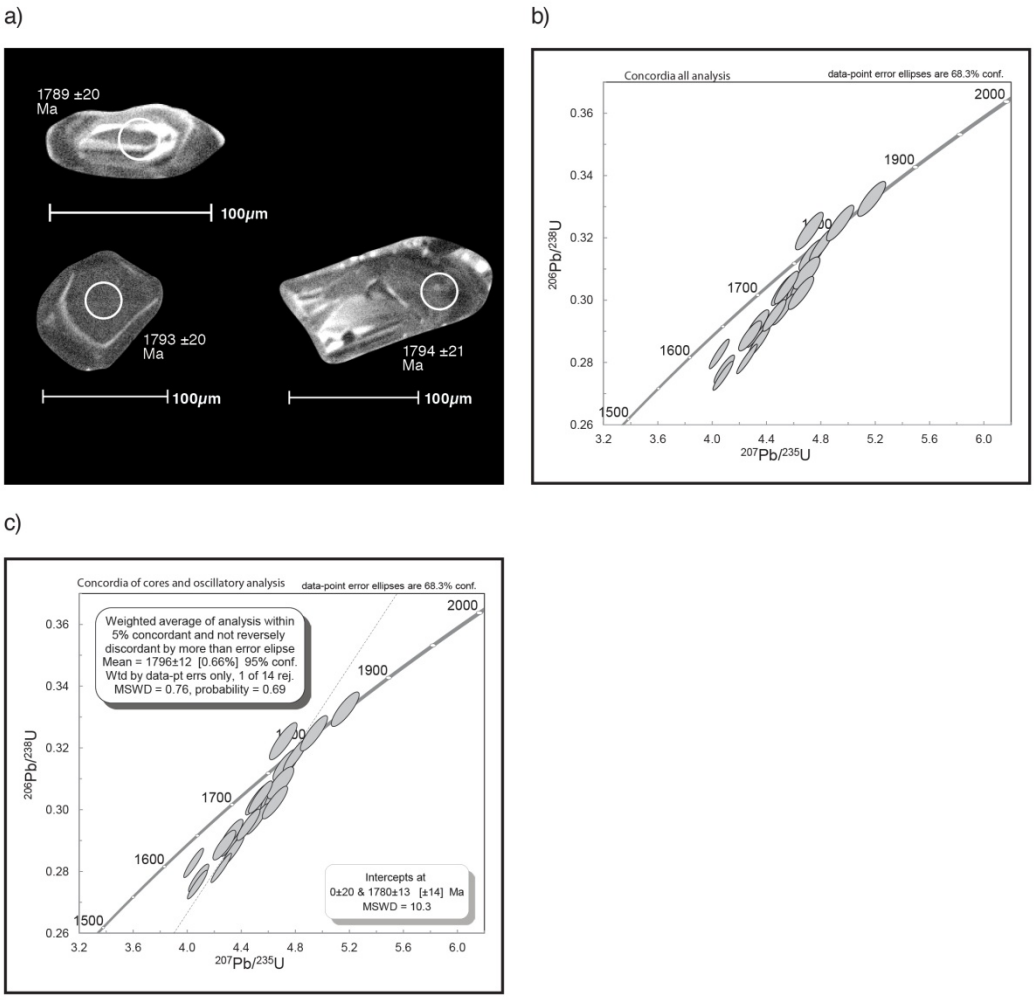

Figure 8 Sample *2012 Boothby 5*. a) Example of CL images with white circles showing positions targeted on LA-ICP-MS with $^{207}Pb/^{206}Pb$ isotope ages shown. b) Concordia plot of all analyses. c) Concordia plot of only cores and oscillatory zones. A weighted average and an intercept age are shown in the inset text boxes.

MEGACRYSTIC ORTHOGNEISS

Two samples of megacrystic orthogneiss, referred to here as the Mt Boothby Orthogneiss (Stewart *et al.* 1980), were analysed; *2012 Boothby 17* and *MB0818*.

The Mt Boothby Orthogneiss is a biotite-plagioclase-Kfeldspar gneiss with minor sporadic garnet which has a biotite defined foliation. Based on both the homogeneity of

the Mt Boothby Orthogneiss at map-scale and the mineral assemblage, the sample is interpreted to have an igneous protolith.

Sample - 2012 Boothby 17

This sample was chosen to provide a minimum constraint on the age of the S_1 fabric in the composite mafic-felsic gneiss. At the sampled locality, the granitic protolith had intruded and truncated the gneissic fabric within the composite mafic-felsic (Figure 3a). Zircon morphology is euhedral-subhedral and elongate with aspect ratios ranging from 3:1 to 2:1 and size from 80-150 µm (Figure 9). Many zircons are dark, diffuse or homogeneous but preserved oscillatory zonation is clearly present in some grains. Small dark rims, 1-10 µm in width, are visible on some grains and however these were too small to be reliably analysed.

In total forty analyses were taken from sample *2012 Boothby 17*. A weighted average age of 1788±15 Ma (MSWD = 1.3) was obtained from fifteen analysis targeting oscillatory zoned zircons. Although many of the grains were discordant a good fit for a concordia intercept age was not possible.

The fifteen analyses used for the weighted average age were isolated from a smaller population of ages of four zircons with a weighted average of 1875±26 Ma using the 'Unmix ages' algorithm (Sambridge & Compston 1994) in Isoplot (Ludwig 2003). The group of four are interpreted to be inherited zircons except for analysis '30R' which is located on a rim of a grain with a core analysis with an age of 1811 Ma.

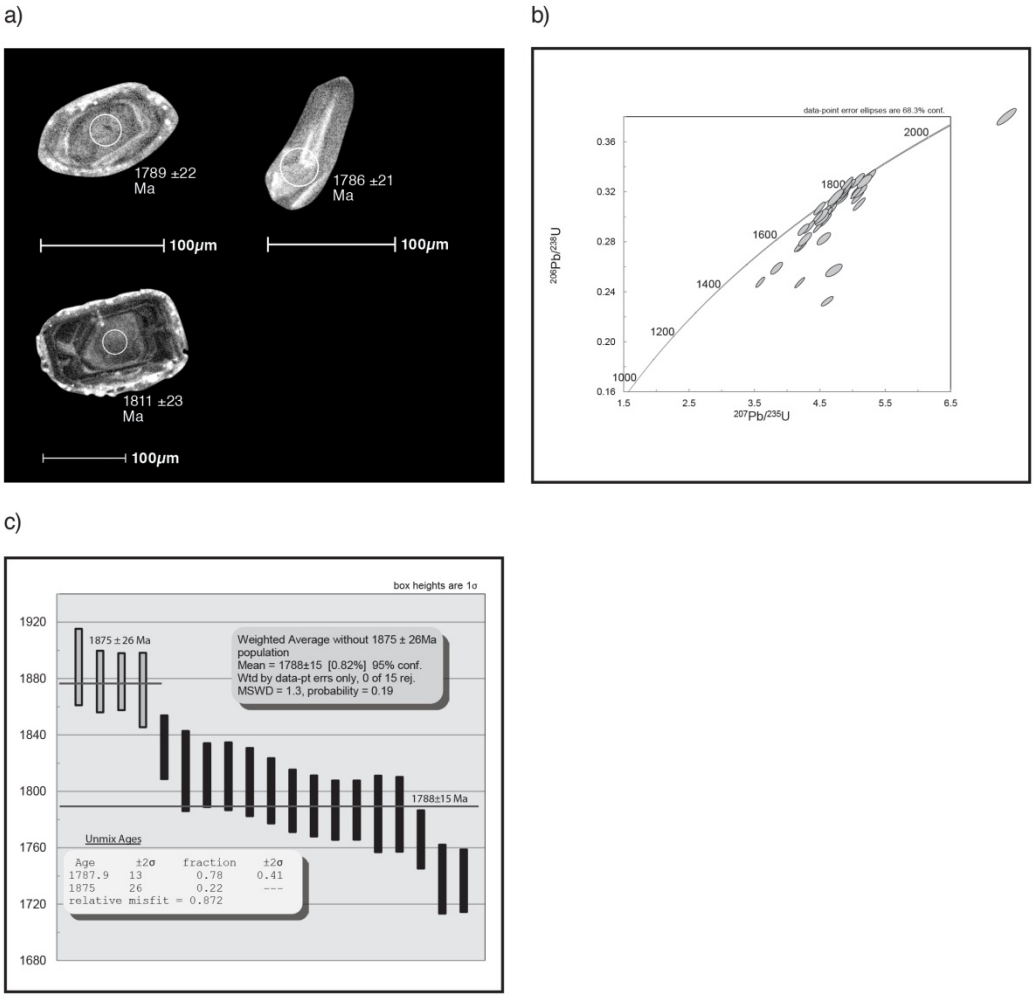

Figure 9 Sample *2012 Boothby 17* a) Example of CL images with white circles showing positions targeted on LA-ICP-MS with ^{207}Pb /^{206}Pb isotope ages shown. b) Concordia plot of all analyses. c) An age density plot showing two distinct populations and their weighted averages.

Sample - MB0818

Sample *MB0818* is a garnet-sillimaitre bearing augen gneiss. In constrast to '2012 Boothby 17', this sample is structurally more complex and contains a transposed migmatitic foliation and was therefore sampled to see if it was significantly different in age to the less structurally complex orthogneiss.

Zircon morphology is euhedral-subhedral with elongate grains with aspect ratios generally 3:1 – 4:1 with some shorter round zircons closer to 2:1 (Figure 10). The

zircons range from 90 – 250 μm in length. The zircons consist of a balance of well defined bright-dark oscillatory zoning with some darker diffuse and metamict grains. The cores of the oscillatory zones are generally brighter than surrounding rims which also generally show oscillatory zoning. Thin dark rims, 1-10 μm in width, cut oscillatory zones in some grains. Some central cores show an irregular shape with less distinct zoning compared to the rest of the surrounding grain. These grains are often considerably darker or lighter than the rest of the grain and are interpreted to be inherited grains.

In total eighty-four analyses were taken from sample *MB0818* however thirty-seven analyses were from grains that were either metamict or ambiguous in their morphology when CL images were reviewed. A weighted average $^{207}Pb/^{206}Pb$ age of 1794.7±8.5 Ma (MSWD = 0.77) is calculated from 29 analyses that targeted oscillatory zoned zircons.

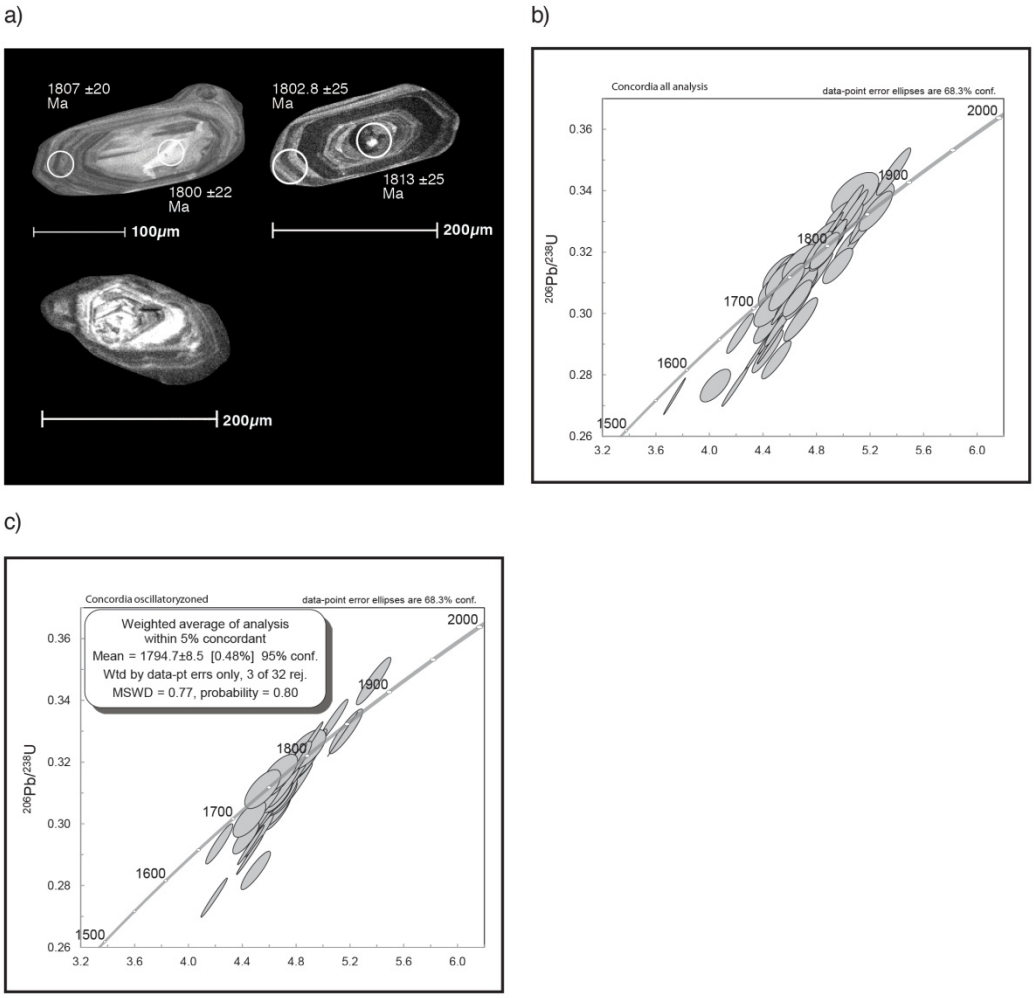

Figure 10 Sample *MB0818* a) Example of CL images with white circles showing positions targeted on LA-ICP-MS with ^{207}Pb /^{206}Pb isotope ages shown. b) Concordia plot of all analyses. c) Concordia plot of only cores and oscillatory zones. A weighted average and is shown in the inset text box.

METASEDIMENTARY GNEISSES

Two samples of cordierite-sillimanite-biotite-K-feldspar-ilmentite-quartz metasedimentary gneiss have been analysed; *2012 Boothby 12* and *Boothby OSM*. They exhibit a foliation defined by biotite which is interpreted to be a composite $S_0/S_1/S_2$ fabric.

Sample - 2012 Boothby 12

Sample *2012 Boothby 12* is taken from the metasedimentary unit immediately adjacent to the composite mafic-felsic gneiss near the summit of Mt Boothby (Figure 2) and was selected to attempt to determine an affinity with known sedimentary packages in the Reynolds Range region (Claoué-Long *et al.* 2008a).

Zircon morphology is euhedral-subhedral often with euhedral grains surrounded by subhedral metamorphic overgrowth (Figure 11). The aspect ratio is most commonly 2:1, occasionally 3:1 or 1:1, with some needle-like grains 4:1. In general the longer grains show more prominent oscillatory zonation with the shorter grains more often diffuse. Particularly thin well defined oscillatory zoning is commonly associated with $^{207}Pb/^{206}Pb$ ages ranging from 1740 Ma – 1830 Ma where as diffuse dark or subtle zonation is more common in the 1550 – 1600 Ma grains. Irregular shaped core fragments are often associated with older $^{207}Pb/^{206}Pb$ ages however their textures are variable.

A cumulative frequency plot (Figure 11c) for all analyses within 5% concordant shows a prominent peak at 1830 Ma, with a small deviation at 1747 Ma and another peak at 1580 Ma, this population consisting of nine samples has a U-Pb $^{207}Pb/^{206}Pb$ weighted average of 1581±15 Ma (MSWD = 0.82).

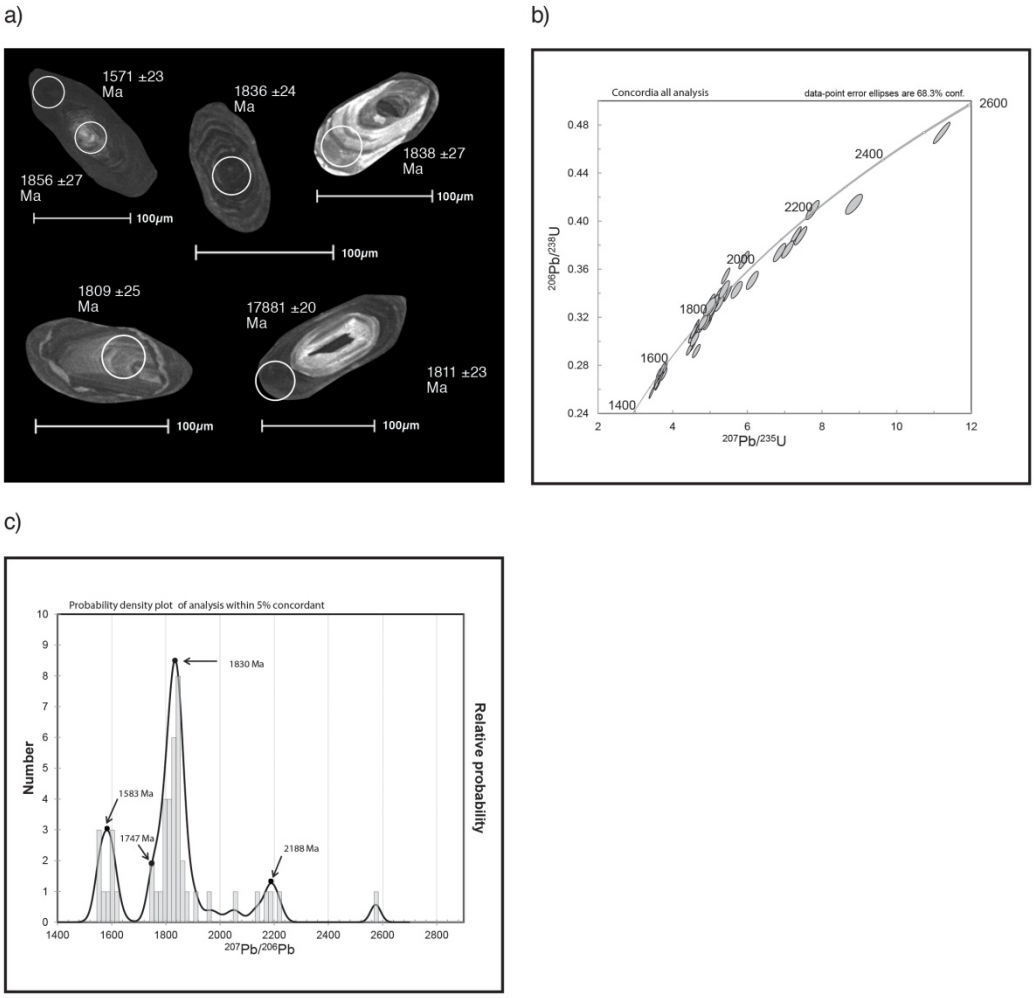

Figure 11 Sample *2012 Boothby 12*. a) Example of CL images with white circles showing positions targeted on LA-ICP-MS with ^{207}Pb /^{206}Pb isotope ages shown. b) Concordia plot of all analyses. c) Cumulative frequency plot of all analyses within 5% concordant.

Sample - Boothby OSM

The *Boothby OSM* sample is a representative metasedimentary with a cordierite-biotite-sillimanite-Kfeldspar-quartz-ilmenite assemblage. Zircon morphology is similar to '2012 Boothby 12' with shorter round zircons with a 2:1 and 1:1 aspect ratio more prominent (Figure 12). Oscillatory banding is not as fine as in *2012 Boothby 12* and ages of well defined light oscillatory banding tend to be associated with slightly older ages predominantly around 1860 Ma. Darker oscillatory zoning is more common with

the 1810-1720 Ma grains whilst irregular shaped cores with variable textures are generally associated with the grains older than 1900 Ma.

A cumulative frequency plot (Figure 12c) for all analyses within 5% concordant shows a prominent peak at 1850 Ma, which is interpreted to be the maximum depositional age of the sedimentary protolith.

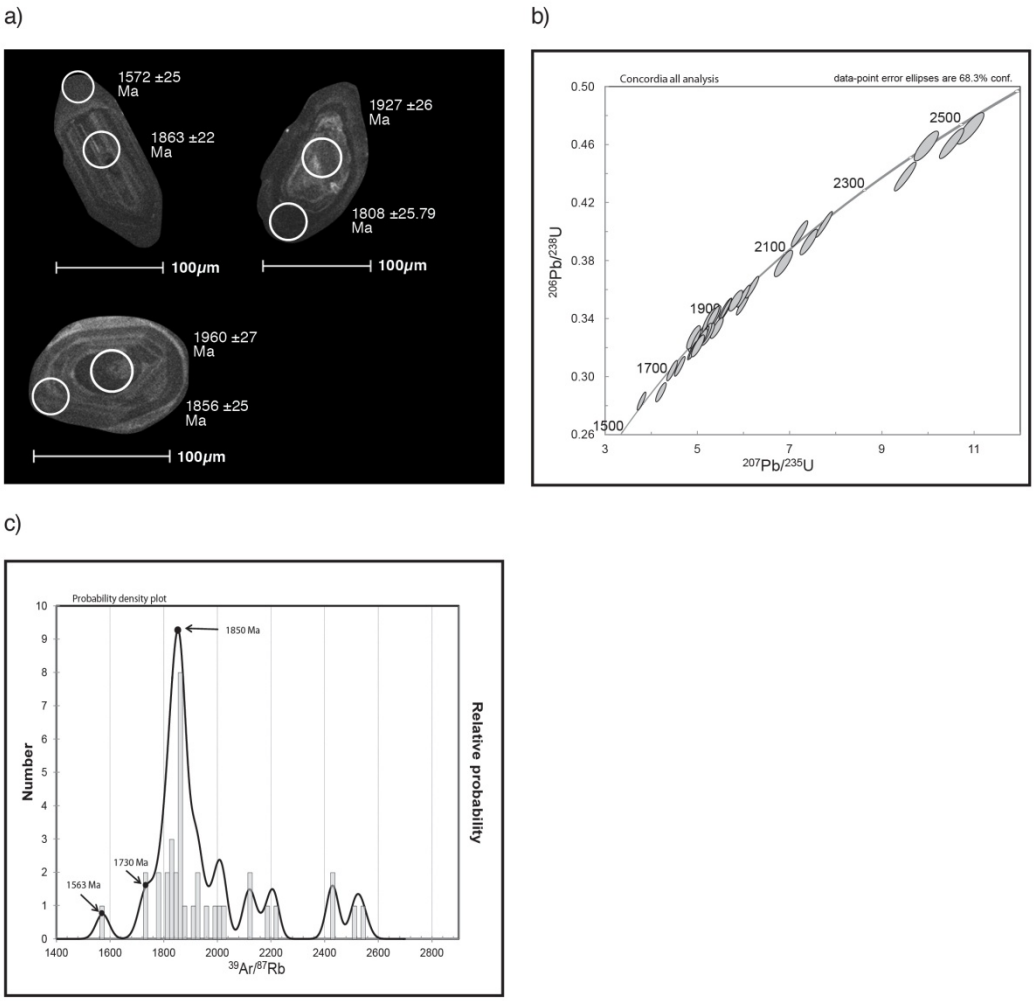

Figure 12 Sample *Boothby OSM*. a) Example of CL images with white circles showing positions targeted on LA-ICP-MS with ^{207}Pb /^{206}Pb isotope ages shown. b) Concordia plot of all analyses. c) Cumulative frequency plot of all analyses within 5% concordant.

MICROGRANITE DYKE

Sample *2012 Boothby 14* is a fine grained unfoliated felsic micro-granite dyke (Figure 3f) that cuts the composite S_1/S_2 fabric in the composite felsic-mafic gneiss and was chosen to constrain the minimum age of the S_1/S_2 foliation.

The zircon CL response was extremely poor in this sample. The BSE imaging was used to distinguish monazite grains, which appear brighter in BSE imaging, from zircon grains which are lower contrast and the laser was fired 'blind' to the center of the zircon. The zircon are euhedral-subhedral grains between 50-120 µm in size with aspect ratios generally 2:1 with some 3:1 and some approaching 1:1.

A total of twenty-four analyses were made. A weighted average $^{207}Pb/^{206}Pb$ age of 1573±15 Ma (MSWD = 0.33) and an upper intercept age of 1577±9 Ma (MSWD = 1.7) are calculated for twelve and nineteen analyses respectively (Figure 13). The intercept age was calculated with four outlying analyses removed, shown in black on Figure 13b, to isolate what appears to be a clear population.

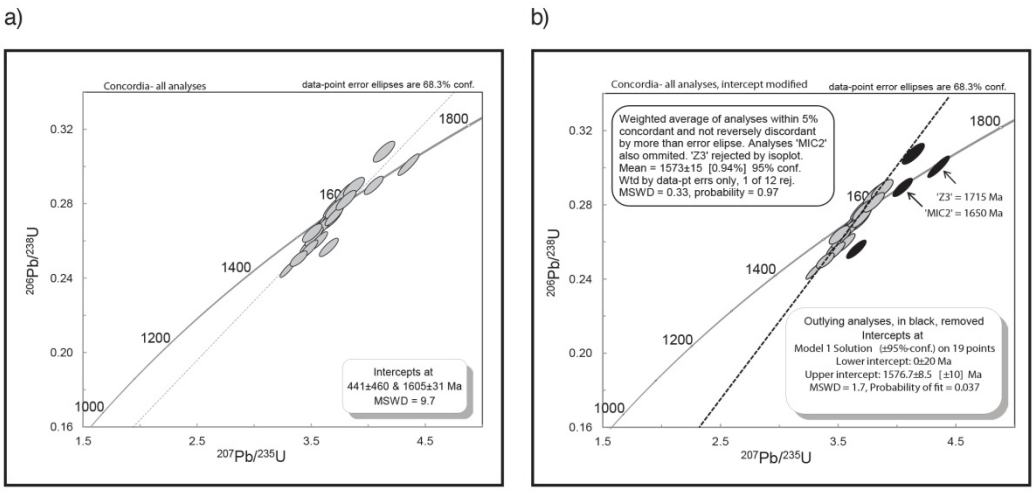

Figure 13 Sample *2012 Boothby 14*. a) Concordia plot of all analyses. b) A modified concordia plot with four grains exempted. Inset boxes show a weighted average age and an concordia intercept age.

U-Pb monazite geochronology

MEGACRYSTIC ORTHOGNEISS

Sample - 2012 Boothby 17

Monazite grains from *2012 Boothby 17* are anhedral, showed generally weak and diffuse compositional zones in BSE imaging and were commonly fractured. Sizes ranged from 60 -140 µm. No pattern of age data was reconciled with compositional zones. Sixteen analyses give a $^{207}Pb/^{206}Pb$ weighted average of 1553±10 Ma (MSWD = 0.98; Figure 14).

Sample - MB0818

Monazites from sample *MB0818* are subhedral to rounded showing patchy weak compositional zonation in places ranging in size from 80 – 200 µm. Often unfractured and with well defined smooth grain boundaries, however some grains are fractured either from grain edges or occasionally radially from the grain center. No pattern of age data was reconciled with compositional zones.

Sample *MB0818* gives a weighted average $^{207}Pb/^{206}Pb$ age of 1534±10Ma (MSWD = 1.15) from fifteen analyses within a distinct population. Another four analysis which are within 5% concordant give $^{207}Pb/^{206}Pb$ ages between 1707 Ma and 1761 Ma (Figure 14).

METASEDIMENTARY GNEISSES

Sample - 2012 Boothby 12

Monazite grains from *2012 Boothby 12* were highly fractured and subhedral ranging in size from 50-120 µm. No compositional zoning was evident in the BSE images. Seventeen analyses gave a $^{207}Pb/^{206}Pb$ weighted average age of 1549±10 Ma (Figure 14).

Sample - Boothby OSM

Monazite grains for *Boothby OSM* ranged from highly fractured internally and along grain boundaries to well defined fresh grains. When fresh the grains appear subhedral-rounded with weak compositional zoning and ranging in size from 100-300 µm. No pattern of age data was reconciled with compositional zones. A total of 19 analysis were taken giving a $^{207}Pb/^{206}Pb$ weighted average age of 1551±9 Ma (Figure 14).

MICROGRANITE DYKE

Sample *2012 Boothby 14* Monazite grains were highly fractured subhedral-rounded with patchy compositional zoning and ranging in size from 40 – 100 µm. The data is highly discordant (Figure 14) but gives a concordia intercept age of 1523±28 Ma (MSWD = 6.4) with a lower intercept, calculated by isoplot, suggesting that resetting was related to the c. 450 -300 Ma Alice Springs Orogeny (Raimondo *et al.* 2011).

a) *2012 Boothby 17*

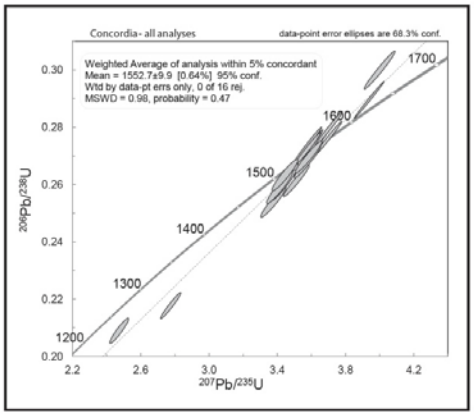

b) *MB0818*

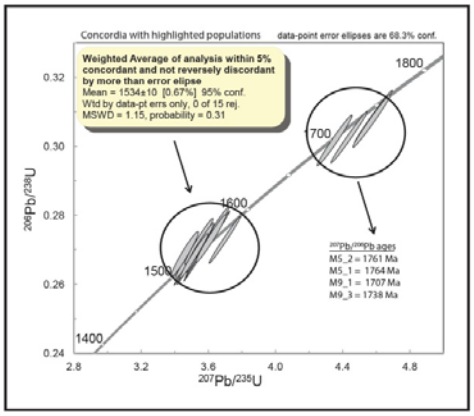

c) *2012 Boothby 12*

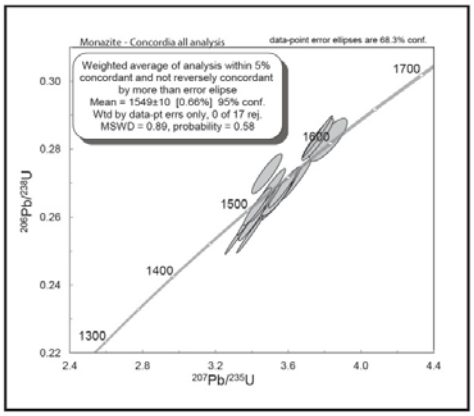

d) *Boothby OSM*

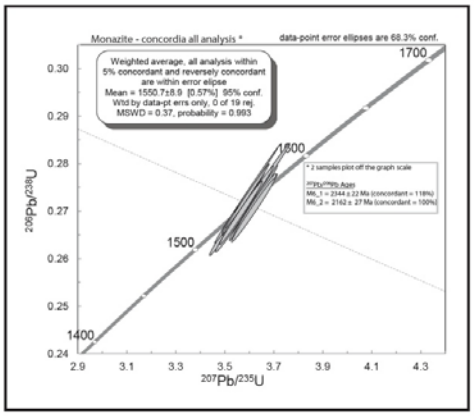

e) *2012 Boothby 14*

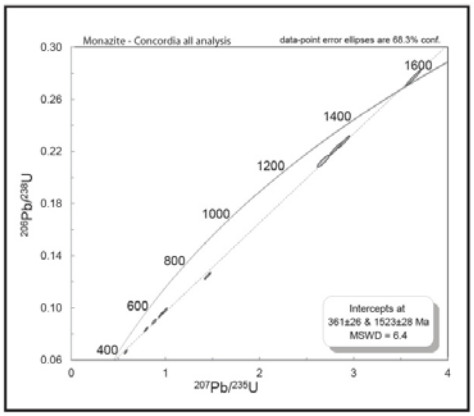

Figure 14 Geochronology results for all monazite analyses. a) A concordia plot showing all analyses for sample *2012 Boothby 17*. b) A concordia plot showing all analyses for sample *MB0818* with two distinct populations highlighted with an inset box showing the weighted average age for the younger population and individual ages listed for the older grains. c) Concordia plot showing all analyses for sample *2012 Boothby 12* with a weighted average in the inset box. d) Concordia showing all analyses for sample *Boothby OSM* with a weighted average age in inset box and ages of two grains that plot off the graph. e) Concordia plot of all analyses from sample *2012 Boothby 14* with a calculated intercept age in the inset box.

P–T PSUEDOSECTION CALCULATIONS

The *P–T* modelling in this study is preliminary and aimed at providing a generalised picture of the thermobarometric regime. Detailed thermobarometric modelling, compositional and *P–T* path matching is beyond the scope of this study. For *P–T* psuedosection methods see Appendix D. Petrographic observation showed that the assemblage for the *Boothby OSM* is cordierite-biotite-sillimanite-K-feldspar-quartz-ilmenite. The calculated PT pseudosection for the *Boothby OSM* is shown in Figure 15. The interpreted stable mineral assemblage for *Boothby OSM* is Kspar-plagioclase-ilmenite-biotite-cordierite-liquid-sillimanite-quartz which is constrainged to 700-800 °C and 3–5.2 kbar.

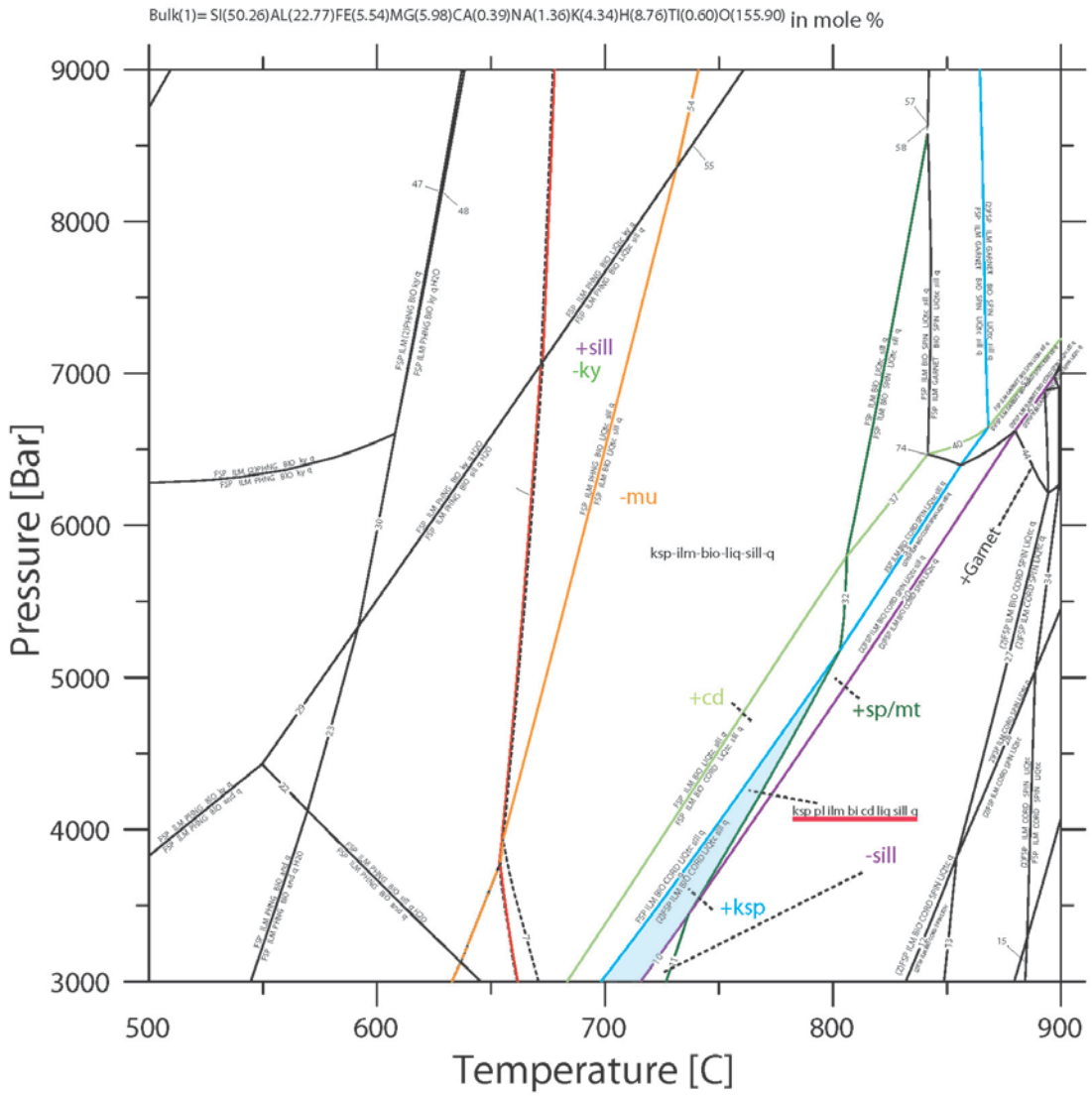

Figure 15 Pressure temperature pseudosection for the *Boothby OSM* sample. The interpreted stable peak metamorphic assemblage is highlighted in blue.

DISCUSSION

Interpretation of the zircon and monazite U-Pb geochronology

COMPOSITE MAFIC-FELSIC GNEISS

The four samples obtained from the composite mafic–felsic gneiss give U-Pb ^{207}Pb-^{206}Pb ages of 1773±6 Ma, 1772±10 Ma, 1789±13 Ma and 1796±12 Ma respectively.

In samples *2012 Boothby 3 – mafic* and 2012 *Boothby 3 – leucocratic* analysed zircon core domains show well developed oscillatory zoning (Figure 5) which is typically associated with growth during magmatic crystallisation (Corfu *et al.* 2003) and therefore these ages are interpreted as protolith ages. In sample *2012 Boothby 4* and *2012 Boothby 5* the majority of grains show a diffuse texture. Although oscillatory zoning is still present in some grains it is much more subtle in comparison with the *2012 Boothby 3* samples. The dark, diffusely zoned, to homogeneous nature of the majority of the zircons is typical of grains that have experienced recrystallisation during metamorphism (Roberts & Finger 1997, Schaltegger *et al.* 1999, Rubatto *et al.* 2001). Rims in all samples, whilst present, were either too small to target, did not show definitive metamorphic overgrowth textures (Roberts & Finger 1997, Schaltegger *et al.* 1999, Corfu *et al.* 2003) or were too discordant to yield definitive ages, although in *2012 Boothby 3 – felsic*, it is evident that new zircon growth occurred at around 1580 Ma.

Given the similarity in ages and the dark/diffuse zircon textures (Figure 7 and 8) seen in CL imaging, it is conceivable that samples *2012 Boothby 4* and *2012 Boothby 5* are the result of metamorphism at around 1790 Ma with the ca. 1773 Ma age from '2012 Boothby 3' representing a younger phase of magmatism. In an attempt to better constrain the age of this possible early metamorphism, combining samples '2012 Boothby 4' and *2012 Boothby 5* gives a combined U-Pb $^{207}Pb/^{206}Pb$ weighted average of 1792±8 Ma (MSWD = 1.01). The intrusion of the Mt Boothby Orthogneiss at around 1790 Ma could have been associated with metamorphic zircon resetting in the composite mafic-felsic at 1792±8 Ma. This interpretation would suggest an extended period of magmatism and a complex lithologic amalgamation of intrusive phases in the

composite felsic-mafic. The presence of both a meta-gabbro within the composite mafic-felsic gneiss (Figure 2) and a more felsic unit at the margin (Figure 2) may indicate magmatic phases from an evolving magmatic system. An alternative interpretation would be that the error margins on the results overlap enough to assume that the composite mafic-felsic gneiss protolith was a single magmatic episode and the intrusion of the protolith of the Mt Boothby Orthogneiss occured shortly after, within the same overlapping error window.

MEGACRYSTIC ORTHOGNEISS

Two samples of the Mt Boothby Orthogneiss, *2012 Boothby 17* and *MB0818,* gave U-Pb ^{207}Pb-^{206}Pb ages of 1788±15 Ma and 1795±8 respectively. These ages are associated with zircon morphologies that show core domains with developed oscillatory zoning (Figure 9 & 10) suggesting growth during magmatic crystallisation (Corfu *et al.* 2003). The most important of these three samples is *2012 Boothby 17* (1788±15 Ma) as this sample was collected where the intrusive relationship with the already foliated composite felsic-mafic was clearly evident (Figure 3a).

Both the *2012 Boothby 17* and *MB0818* samples were also analysed to obtain monazite U-Pb ^{207}Pb/^{206}Pb ages which give pooled U-Pb ^{207}Pb/^{206}Pb age of 1553±10 Ma and 1534±10 Ma respectively. The lack of other substantial data indicating metamorphic zircon growth prior to ~1550 Ma and after the calculated magmatic age of 1773±6 Ma for the composite mafic-felsic gneiss suggests that the S_2 foliation within the Mt Boothby Orthogneiss developed during the Chewings Event, which occurred between 1590 – 1540 Ma (pers. comm. Morrissey, 2012; Hand and Buick 2001). By inference this also corresponds to the timing of the isoclinal F_2 folding within the composite

mafic-felsic gneiss, because the orthogneiss only records one phase of pervasive foliation development, whereas the composite mafic-felsic gneiss records two phases.

METASEDIMETARY GNEISSES

The cumulative frequency plots for the metasediment samples *Boothby OSM* and *2012 Boothby 12* suggest that the sedimentary protoliths were deposited after 1858 Ma and 1830 Ma respectively. Comparisons of the detrital zircon age spectra of the *Boothby OSM* and *2012 Boothby 12* samples with those of the Lander Package and Reynolds Range Group (Figure 16) suggest that the Mt Boothby metasediments share provenance affinities with the Lander Package rather than the Reynolds Range Group (Claoué-Long *et al.* 2008a).

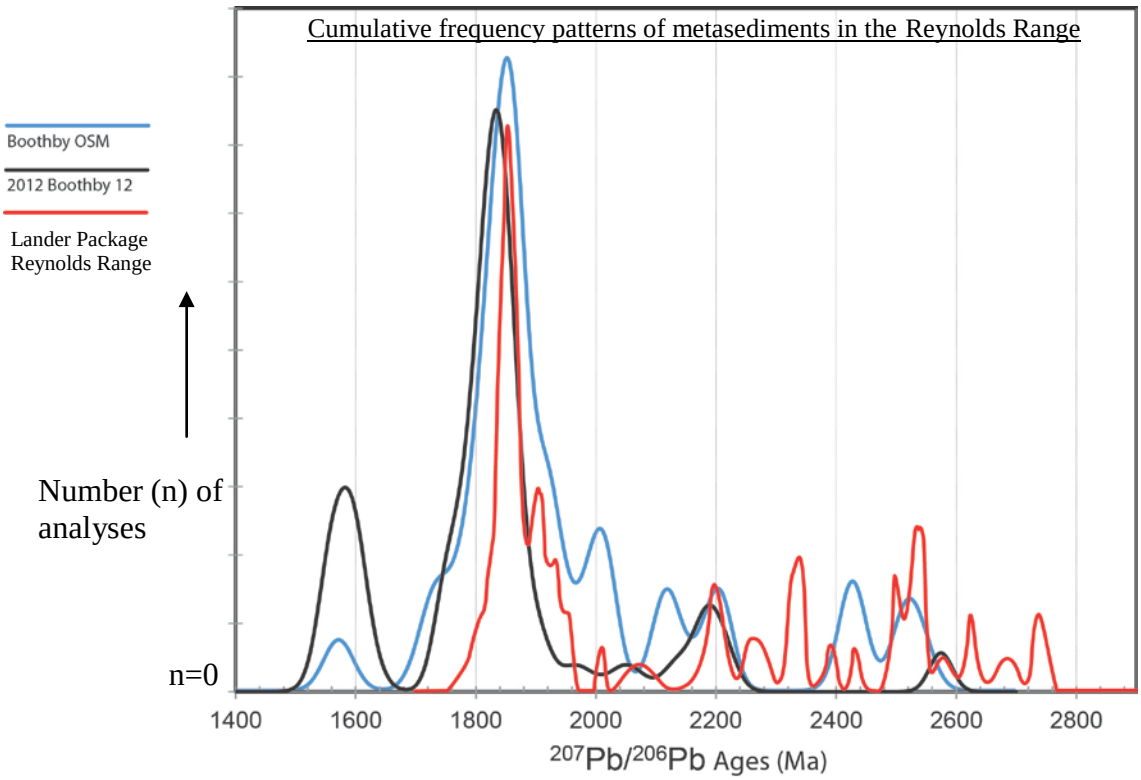

Figure 16 Comparison of cumulative frequency plot patterns of metasedimentary rocks in this study, *Boothby OSM* and *2012 Boothby 12* with an established Lander Package cumulative frequency plot (Claoué-Long *et al.* 2008a). Clear similarities are shown between peaks at 1830-1850 Ma, 2200 Ma and 2550-2575 Ma.

Clear intrusive relationships were not established with any of the adjacent igneous lithologies and they also lack any clearly transposed fabrics or associated isoclinal folding. It is therefore possible that the sediments were deposited later than the igneous rocks. Kinks in the cumulative frequency plots from both of the metasedimentary samples in this study at 1730 Ma and 1747 Ma may in fact indicate the youngest detrital grains. However, it is possible that these could simply be partially reset grains. Without further investigation the interpretation here is that they are most likely related to the Lander Package.

Age constraints on metamorphism and deformation

The age constraints obtained in this study combined with recently acquired monazite U-Pb ages from McBride (2010) and Morrissey (pers. comm., 2012) place well defined constraints on the timing of deformation and high-grade metamorphism in the Mt Boothby area of the eastern Reynolds Range. The age constraints from the Mt Boothby region also allow comparisons to be made with areas further west in the Reynolds Range (Rubatto et al., 2001; Vry et al., 1996; Williams et al., 1996) that build up a regional picture of the timing of deformation and metamorphism.

The foliation in the Mt Boothby Orthogneiss forms part of a map scale tectonic fabric (Figure 2) that is parallel to primary lithological layering. In the metasedimentary lithologies, particularly those around grid reference 0324817E 7502155N (Figure 4) this regional foliation is parallel to the axial surface of isoclinal folding which itself is defined by both the primary lithological layering and a high-grade metamorphic foliation. From this structural relationship it can be inferred that primary lithologic layering (bedding – S_0) has been associated with the formation of a high grade

metamorphic foliation (S_1). Subsequently the composite S0/S1foliation underwent isoclinal F_2 folding.

In the composite mafic-felsic gneiss there is also extensive evidence for poly-deformation with abundant cm-m-scale isoclinal folds defined by a migmatitic gneissic foliation (Figure 2 & 3a,b,c,d). The structural complexity of the composite mafic-felsic gneiss contrasts with the simple deformational style in the Mt Boothby Orthogneiss, whose protolith intruded the composite mafic-felsic gneiss. While the contrast in structural complexity could again reflect patterns of strain partitioning (Clegg and Holdsworth, 2005; Holdsworth et al., 2002), the intimate association of the two rock units, and the locally intrusive relationships (Figure 3a,b,c,d), suggest that the composite felsic-mafic was already deformed and metamorphosed prior to the intrusion of the Mt Boothby Orthogneiss protolith. In this case the U-Pb age data obtained in this study can be used to constrain the timing of early high-grade deformation in the Mt Boothby area with the 1792±8 Ma metamorphic zircons in samples '2012 Boothby 4' and '2012 Boothby 5' recording the age of deformation. The 1792±8 Ma age proposed is broadly synchronous with the Yambah Event whose affects are best recorded in the southern Arunta region (Claoué-Long & Hoatson 2005), as well as voluminous felsic magmatism further west in the Reynolds and Anmatjira Ranges (Hand & Buick 2001). Sample 'MB0818' also returned four monazite ages ranging from 1707–1764 Ma raising the possibility of another metamorphic event occurring within this timeframe. Although there is a lack of conclusive evidence for an event at this time in individual samples the entire data set of this study does lend some support. Cumulative frequency plots from the metasedimentary gneisses *2012 Boothby 12* and *Boothby OSM* show deviations at 1747 Ma and 1730 Ma respectively. Furthermore, zircon analyses of

oscillatory zones or rims in each of the composite mafic-felsic gneiss samples and Mt Boothby Orthogneiss samples commonly extend to 1720-30 Ma. In *2012 Boothby 3 – mafic* two concordant analyses of rims are at 1741±20 Ma and 1736±19 Ma. Another two concordant analyses from oscillatory zones are recorded at 1729±21 and 1745±21. Similarly in the other six samples from the composite mafic-felsic gneiss and Mt Boothby Orthogneiss a total of 11 analyses record U-Pb $^{207}Pb/^{206}Pb$ ages between 1750 Ma and 1700 Ma, generally between 1720-40 Ma. This makes a total of 15 concordant analyses from 173 total concordant analyses of core/oscillatory and rim domains representing approximately 8.5% of the sample selection. If these zircon ages were the result of partial resetting by Chewings-aged metamorphism this would likely result in a smear of near concordant ages zircons ages being drawn along concordia (Halpin et al., 2012) to approx 1550 Ma. However there is a clear gap between the ages that track down to 1730 and later Chewings, <1600 Ma ages. This suggests that zircons ages around 1730 Ma might have either been the result of recrystallisation at that time or have been drawn along concondia to an event at around 1730 Ma.

McBride (2010) and Morrissey (pers. comm., 2012) have obtained a number of monazite U-Pb ages between 1575-1540 Ma from granulite facies metasedimentary samples from the Mt Boothby region. These ages are similar, although ranging to slightly younger, to ages obtained from metamorphic zircon and monazite from granulite facies metasediments in Reynolds Range ~ 20 km west of Mt (Vry *et al.* 1996, Williams *et al.* 1996, Rubatto *et al.* 2001, Reid 2012).These ages have been interpreted to reflect the timing of regional deformation and high-grade metamorphism in the Reynolds Range. These early Mesoproterozoic monazite and zircon U-Pb ages are similar to the monazite age of 1549±10 Ma obtained from the foliated orthogneiss

sample ‘2012 Boothby 17’ whose protolith is interpreted to have intruded the composite mafic-felsic gneiss (Figure 3 a,b,c,d,) around 1773-1782 Ma. The foliated orthogneiss contains a simple foliation that appears to record only one phase of deformation, and it is suggested here that this deformation is early Mesoproterozoic in age, and part of the regional-scale Chewings Event, 1590 Ma – 1570 Ma, that affected the adjacent Reynolds and Anmatjira Ranges (Hand and Buick, 2001; Rubatto et al., 2001; Vry et al., 1996; Williams et al., 1996). Further constraining the age of deformation associated with Chewings Event is the interpreted ~ 1575 Ma protolith age of the micro-granite dyke obtained in this study. Given that this rock cuts the S_2 fabric in the Mt Boothby Orthogneiss it must have intruded post S_2 formation. If the S_2 foliation is accepted to be Chewings-aged, based on the bulk of monazite age data between ~ 1575 – 1540 Ma (McBride, 2010; pers. comm. Morrissey, 2012; this study), then the age from the microgranite constrains foliation formation to early Chewings, conservatively between ~ 1570-1600 Ma, with monazite growth continuing for up to another ~ 30 Ma.

Regional event correlations

This study has identified two major phases of tectonism in the Mt Boothby region, c. 1800-1770 Ma, and c. 1575-1540 Ma. Additionally there appears to be evidence that thermal events may have affected the region at approximately 1740-1730 Ma.

The ages from the composite felsic-mafic gneiss and the Mt Boothby Orthogneiss suggest magmatism was related to the Yambah Event (Giles *et al.* 2002, Claoué-Long & Hoatson 2005). During the Yambah Event felsic and mafic magmatism has been well documented (Hand & Buick 2001, Claoué-Long & Hoatson 2005). The Attutra Metagabbro in the eastern Aileron Province, igneous protoliths to the Mt Chapple Metamorphics (1771-1774 Ma) in the southern Aileron Province and the Harry

Anorthostic Gabbro in the south eastern Aileron Province, as well as in the Reynolds and Anmatjira ranges (Collins & Shaw 1995, Hand & Buick 2001, Claoué-Long & Hoatson 2005). The timing of the Yambah Event also corresponds to the emplacement of calc-alkaline granites and mafic rocks in the south eastern Aileron Province that are interpreted to reflect continental margin magmatism (Foden *et al.* 1988, Zhao & McCulloch 1995, Wade *et al.* 2006). Furthermore, the interpretation that the composite mafic-felsic was deformed prior to intrusion of the Mt Boothby Orthogneiss suggests that deformation was associated with the Yambah Event.

Although there are no direct constraints on the age of the F_3 structure, their migmatitic character suggests they are associated with Chewings-aged deformation and may account for the extended period of monazite growth subsequent to D_2 (c. 1575 Ma). The regional foliation appears to be defined primarily by Chewings-aged deformation which was coeval with isoclinal folding (F_2).

Tectonic interpretations of Yambah-aged tectonism in the Mt Boothby region

Claoué-Long and Hoatson (2005) raised the possibility that metamorphism and deformation was associated with Yambah-age magmatism but noted that it was equivocal (Claoué-Long & Hoatson 2005). This study suggests that deformation occurred within the composite felsic-mafic gneiss either during or immediately prior to the Yambah event at ~1792 Ma. The original orientation of the S_1 fabric is unknown due to the intensity of the D_2 deformation. However the map pattern suggests that the F_2 fold interpreted to run through the composite mafic-felsic gneiss has a shallow plunge and it is therefore possible that the original orientation of S_1 was low angle.

The presence of bimodal and calcalkaline magmatism in the Arunta region (Foden *et al.* 1988, Zhao & Bennett 1995, Zhao & McCulloch 1995), which is often related to

magmatic arc systems (Zhao & McCulloch 1995, Wade *et al.* 2006, Clemens *et al.* 2009), has been proposed as evidence for an arc system involved in the crustal evolution of Proterozoic Australia (Giles *et al.* 2002, Betts & Giles 2006, Wade *et al.* 2006). Giles et al. (2002) suggested that the Yambah Event was a period of arc magmatism and backarc extension. The apparent Yambah aged D_1 deformation in the composite mafic-felsic gneiss in the Mt Boothby region and the inference that the S_1 fabric may have been low angle suggests that c. 1790 Ma tectonism in the central Arunta region may have been extensional in character. The inferred timing of this early deformation corresponds, within error, with the deposition of the marine Reynolds Range Group immediately to the west (Claoué-Long *et al.* 2008a). Conceivably the deposition of the Reynolds Range Group was a basinal response to tectonic extension. The inferred age of D_1 deformation in the Mt Boothby region overlaps with the high geothermal gradient 1800 Ma Stafford Event (Collins & Shaw 1995, Hand & Buick 2001, Claoué-Long & Hoatson 2005) suggesting that an extended period of extension, sedimentation, magmatism and deformation occurred at around 1800 Ma in the central Aileron Province.

CONCLUSIONS

Zircon and monazite U–Pb isotope geochronology combined with structural mapping in the Mt Boothby region in the central Aileron Province in Central Australia has constrained the timing of two tectonically distinct phases of high-grade deformation and metamorphism. The first event (D_1/M_1) occurred at around 1790 Ma and coincides with the early stages of the Yambah Event, which is widely recognised in the southern Aileron Province, but has not previously been unequivocally shown to be associated with deformation. Subsequent pervasive reworking occurred over the interval 1600-

1570 Ma. and coincides with the Chewings Orogeny. During the Chewings Orogeny the c.1790 Ma D_1 structures were transposed into a composite S_1/S_2 fabric. Map scale F_2 folding is interpreted to have a shallow plunge suggesting that the S_1 fabric may have originally been shallow dipping, raising the possibility that deformation was extensional in nature, and coeval with deposition of the nearby Reynolds Range Group which is constrained to the interval 1806-1785 Ma. Although inferred here to be Yambah aged, the timing constraints for D_1 /M_1 also overlaps with the c. 1800 Ma Stafford Event which was associated with voluminous felsic magmatism, mafic magmatism and extreme geothermal gradient magmatism. This suggests that an extended period of extension, sedimentation, magmatism and deformation may have occurred at around 1800 Ma in the central Aileron Province.

ACKNOWLEDGMENTS

This project would not have been possible without the fantastic support of my primary supervisor Martin Hand who provided timely and detailed advice throughout the year. Justin Payne, for assistance particularly with the geochronology lab work. David Kelsey who provided detailed feedback on drafts and much of the organisational work for my field work. Katie Howard for assisting with lab bookings, lab training and anything/everything else that needed to be done. The Central Australia honours group, Maddison Lawson-Wyatt, Claire Thomas, Courtney Fields and particularly Matt Reid who assisted me with my field work. The assistance and cooperation within this group was exceptional. Alec Walsh, particularly for his work with the THERIAK-DOMINO program and providing invaluable help with the phase equilibria modelling. PhD students Jade Anderson, Kathleen Lane, Russell Smits, Bonnie Henderson, Laura Morrissey and Diana Plavsa who were always ready to provide help if asked. Tom Raimondo. The dedicated staff at Adelaide Microscopy. John Arnold for assistance with design and layout. My parents Lorraine and Phil Howlett and ALL my extended family who have been so supportive and understanding this year. Special thanks to my partner Kate and our daughters Delilah and Esther, words cannot express. Lastly, the late Nellie Ruth Howlett, without whom my return to study may not have been possible.

This project was funded by ARC discovery project DP1095456 and ARC linkage project LP100200127.

REFERENCES

BETTS P. G. & GILES D. 2006. The 1800–1100 Ma tectonic evolution of Australia. *Precambrian Research* **144**, 92-125.

CAWOOD P. A. & KORSCH R. J. 2008. Assembling Australia: Proterozoic building of a continent. *Precambrian Research* **166**, 1-38.

CLAOUÉ-LONG J., EDGOOSE C. J. & WORDEN K. 2008a. A correlation of Aileron Province stratigraphy in central Australia. *Precambrian Research* **166**, 230-245.

CLAOUÉ-LONG J. & HOATSON D. M. 2005. Proterozoic mafic–ultramafic intrusions in the Arunta Region, central Australia Part 2: Event chronology and regional correlations. *Precambrian Research* **142**, 134-158.

CLAOUÉ-LONG J., MAIDMENT D. W., HUSSEY K. & HUSTON D. 2008b. The duration of the Strangways Event in central Australia: Evidence for prolonged deep crust processes. *Precambrian Research* **166**, 246-262.

CLEMENS J. D., DARBYSHIRE D. P. F. & GFLINDERS J. 2009. Sources of post-orogenic calcalkaline magmas: The Arrochar and Garabal Hill–Glen Fyne complexes, Scotland. *Lithos* **112**, 524-542.

COLLINS W. J. 2002a. Hot orogens, tectonic switching, and creation of continental crust. *Geology* **30; no. 6**, 535-538.

COLLINS W. J. 2002b. Nature of extensional accretionary orogens. *Tectonics* **21**, **6** (1-12).

COLLINS W. J. & SHAW R. D. 1995. Geochronological constraints on orogenic events in the Arunta Inlier: a review. *Precambrian Research* **71**, 315-346.

CORFU F., HANCHAR J. M., HOSKIN P. W. O. & KINNY P. D. 2003. Atlas of zircon textures. *In:* Hanchar J. M. & Hoskin P. W. O. eds., *Zircon*, pp 468-500, Washington, D. C.

DIRKS P. H. G. M., HAND M. & POWELL R. 1991. The P-T-deformation path for a mid-Proterozoic, lowpressure terrane: the Reynolds Range, central Australia. *Journal of Metamorphic Geology* **9**, 641-661.

FODEN J. D., BUICK I. S. & MORTIMER G. E. 1988. The petrology and geochemistry of granitic gneisses from the east arunta inlier, central australia: implications for proterozoic crustal development. *Precambrian Research* **40/41**, 233-259.

GILES D., BETTS P. G. & LISTER G. 2002. Far-field continental backarc setting for the 1.80–1.67 Ga basins of northeastern Australia. *Geological Society of America* **30**, 823-826.

GRIFFIN W. L. & POWELL W. J. 2008. *GLITTER: data reduction software for laser ablation ICP-MS. Laser Ablation ICP-MS in the Earth Sciences: Current Practices and Outstanding Issues. Mineralogical Association of Canada. Short Course Series 40*. 308-311 S.

HAND M. & BUICK I. S. 2001. Tectonic evolution of the Reynolds-Anmatjira Ranges: a case study in terrain reworking from the Arunta Inlier, central Australia. *Continental Reactivation and Reworking*, 237-260.

HOSKIN P. W. O. & SCHALTEGGER U. 2003. The Composition of Zircon and Igneous and Metamorphic Petrogenesis. *In:* Hanchar J. M. & Hoskin P. W. O. eds., *Zircon*, pp 27-62, Washington, D. C.

JACKSON S. E., PEARSON N. J., GRIFFIN W. L. & BELOUSOVA E. 2004. The application of laser ablation-inductively coupled plasmamass spectrometry to in situ U–Pb zircon geochronology. *Chemical Geology* **211**, 47-69.

LUDWIG K. R. 2003. Isoplot 3.00. *Berkeley Geochronology Center Special Publication* **4**.

MAIDMENT D. W. 2005. Palaeozoic high-grade metamorphism within the Centralian Superbasin, Harts Range region, central Australia. *PhD Thesis, Australian National University, Canberra (unpubl.)*.

MAIDMENT D. W., HAND M. & WILLIAMS I. S. 2005. Tectonic cycles in the Strangways Metamorphic Complex, Arunta Inlier, central Australia: geochronological evidence for exhumation and basin formation between two high-grade metamorphic events*. *Australian Journal of Earth Science* **52**, 205-215.

MCBRIDE E. 2010. Mid crustal granulite facies metamorphism in the Reynolds Range, central Australia: physical conditions, duration and potential mechanisms. Honours thesis, Centre for Tectonics Resources and Exploration Geology and Geophysics, School of Earth and Environmental Sciences, The University of Adelaide, Adelaide (unpubl.).

MORRISSEY L. 2012. Adelaide.

PAYNE J. L., BAROVICH K. M. & HAND M. 2006. Provenance of metasedimentary rocks in the northern Gawler Craton, Australia: Implications for Palaeoproterozoic reconstructions. *Precambrian Research* **148**, 275-291.

PAYNE J. L., FERRIS G., BAROVICH K. M. & HAND M. 2010. Pitfalls of classifying ancient magmatic suites with tectonic discrimination diagrams: An example from the Paleoproterozoic Tunkillia Suite, southern Australia. *Precambrian Research* **177**, 227-240.

PAYNE J. L., HAND M., BAROVICH K. M. & WADE B. P. 2008. Temporal constraints on the timing of high-grade metamorphism in the northern Gawler Craton: implications for assembly of the Australian Proterozoic. *Australian Journal of Earth Science* **55**, 623-640.

RAIMONDO T., HAND M. & FAURE K. 2011. Assessing the geochemical and tectonic impacts of fluid–rock interaction in mid-crustal shear zones: a case study from the intracontinental Alice Springs Orogen, central Australia. *Journal of Metamorphic Geology* **29**, 821-850.

REID M. D. 2012. New constraints on Chewings-aged deformation and metamorphism of ca.≥ 1750 Ma crust in the Reynolds Range,central Australia. B. Sc (Honours) thesis, Geology and Geophysics, The University of Adelaide, Adelaide (unpubl.).

ROBERTS M. P. & FINGER F. 1997. Do U-Pb zircon ages from granulites reflect peak metamorphic conditions? *Geology* **25; no. 4**, 319-322.

RUBATTO D., WILLIAMS I. S. & BUICK I. S. 2001. Zircon and monazite response to prograde metamorphism in the Reynolds Range, central Australia. *Contrib Mineral Petrol* **140**, 458-468.

SAMBRIDGE M. S. & COMPSTON W. 1994. Mixture modeling of multi-component data sets with application to ion-probe zircon ages. *Earth and Planetary Science Letters* **128**, 373-390.

SCHALTEGGER U., FANNING C. M., GUNTHER D., MAURIN J. C., SCHULMANN K. & GEBAUER D. 1999. Growth, annealing and recrystallization of zircon and preservation of monazite in high-grade metamorphism: conventional and in-situ U-Pb isotope, cathodoluminescence and microchemical evidence. *Contrib Mineral Petrol* **134**, 186-201.

SCRIMGEOUR I. R., KINNY P. D., CLOSE D. F. & EDGOOSE C. J. 2005. High-T granulites and polymetamorphism in the southern Arunta Region, central Australia: Evidence for a 1.64 Ga accretional event. *Precambrian Research* **142**, 1-27.

SELWAY K., HAND M., HEINSON G. S. & PAYNE J. L. 2009. Magnetotelluric constraints on subduction polarity: Reversing reconstruction models for Proterozoic Australia. *Geology* **37**, 799-802.

SLÁMA J., KOSLER J., CONDON D. J., CROWLEY J. L., GERDES A., HANCHAR J. M., HORSTWOOD M. S. A., MORRIS A., NASDALA L., NORBERG N., SCHALTEGGER U., SCHOENE B., TURBRETT M. N. & WHITEHOUSE M. J. 2008. Plešovice zircon — A new natural reference material for U–Pb and Hf isotopic microanalysis. *Chemical Geology* **249**, 1-35.

SMITHIES R. H. & BAGAS L. 1996. High pressure amphibolite-granulite facies metamorphism in the Paleoproterozoic Rudall Complex, central Western Australia. *Precambrian Research* **83**, 243-265.

STEWART A. J., OFFE L., GLIKSON A. Y., WARREN R. G. & BLACK L. P. 1980. Geology of the Northern Arunta Block, Northern Territory. *Bur. Miner. Resour. Aust*, 63-292.

TEYSSIER C., AMRI C. & HOBBS B. E. 1988. South Arunta Block: The internal zones of a proterozoic overthrust in Central Australia. *Precambrian Research* **40/41**, 157-173.

VRY J., COMPSTON W. & CARWRIGHT I. 1996. SHRIMP II dating of zircons and monazites: reassessing the timing of high-grade metamorphism and fluid flow in the Reynolds Range, northern Arunta Block, Australia. *Journal of Metamorphic Geology* **14**, 335-350.

WADE B. P., BAROVICH K. M., HAND M., SCRIMGEOUR I. R. & CLOSE D. F. 2006. Evidence for Early Mesoproterozoic Arc Magmatism in the Musgrave Block, Central Australia: Implications for Proterozoic Crustal Growth and Tectonic Reconstructions of Australia. *The Journal of Geology* **114**, 43-63.

WHITE R. W., POWELL R. & CLARKE G. L. 2003. Prograde Metamorphic Assemblage Evolution during Partial Melting of Metasedimentary Rocks at Low Pressures: Migmatites from Mt Stafford, Central Australia. *Journal of Petrology* **44**, 1937-1960.

WILLIAMS I. S., BUICK I. S. & CARTWRIGHT I. 1996. An extended episode of early Mesoproterozoic metamorphic fluid flow in the Reynolds Range, central Australia. *Journal of Metamorphic Geology* **14**, 29-47.

ZHAO J. & BENNETT V. C. 1995. SHRIMP U-Pb zircon geochronology of granites in the Arunta Inlier, central Australia: implications for Proterozoic crustal evolution. *Precambrian Research* **71**, 17-43.

ZHAO J. & MCCULLOCH T. 1995. Geochemical and Nd isotopic systematics of granites from the Arunta Inlier, central Australia: implications for Proterozoic crustal evolution. *Precambrian Research* **71**, 265-299.

APPENDIX A: FULL GEOCHRONOLOGY DATA SETS

See separate PDF

APPENDIX B: PETROGRAPHIC PHOTOS

See separate PDF

APPENDIX C: FULL GEOCHRONOLOGY METHOD

See separate PDF

APPENDIX D: PT PSUEDOSECTION METHODS AND CALCULATIONS

See separate PDF

APPENDIX E: WHOLE ROCK COMPOSITION DATA FOR BOOTHBY OSM

See separate PDF